OPEN ACCESS

Journal of Statistical Mechanics: Theory and Experiment
An IOP and SISSA journal

PAPER: Quantum statistical physics, condensed matter, integrable systems

The quantum XY chain with boundary fields: finite-size gap and phase behavior

Aldo Coraggio[1] **and Andrea Pelissetto**[2,*]

[1] SISSA, Via Bonomea 265, I-34136 Trieste, Italy
[2] Dipartimento di Fisica di Sapienza, Università di Roma INFN, Sezione di Roma I, Piazzale A. Moro 2, I-00185 Roma, Italy
E-mail: acoraggi@sissa.it and Andrea.Pelissetto@roma1.infn.it

Received 16 May 2024
Accepted for publication 21 October 2024
Published 4 February 2025

Online at stacks.iop.org/JSTAT/2025/023101
https://doi.org/10.1088/1742-5468/ad8bb7

Abstract. We present a detailed study of the finite-size one-dimensional quantum XY chain in a transverse field in the presence of boundary fields coupled with the order-parameter spin operator. We consider fields located at the chain boundaries that have the same strength and that are oppositely aligned. We derive exact expressions for the gap Δ as a function of the model parameters for large values of the chain length L. These results allow us to characterize the nature of the ordered phases of the model. We find a magnetic (M) phase ($\Delta \sim \mathrm{e}^{-aL}$), a magnetic-incommensurate (MI) phase ($\Delta \sim \mathrm{e}^{-aL} f_{\rm MI}(L)$), a kink (K) phase ($\Delta \sim L^{-2}$) and a kink-incommensurate (KI) phase ($\Delta \sim L^{-2} f_{\rm KI}(L)$); $f_{\rm MI}(L)$ and $f_{\rm KI}(L)$ are bounded oscillating functions of L. We also analyze the behavior along the phase boundaries. In particular, we characterize the universal crossover behavior across the K-KI phase boundary. On this boundary, the dynamic critical exponent is $z = 4$, i.e. $\Delta \sim L^{-4}$ for large values of L.

Keywords: integrable spin chains and vertex models, quantum phase transitions, solvable lattice models, spin chains, ladders and planes

*Author to whom any correspondence should be addressed.

Contents

J. Stat. Mech. (2025) 023101

1. Introduction

Understanding how classical or quantum many-body systems order under the action of an external field is an important problem in condensed-matter physics. These ordering phenomena are signaled by phase transitions which, in classical or quantum settings, can be broadly classified into two categories. First, there are continuous transitions characterized by long-range correlations decaying generically as powers of the distance and by universal large-scale behavior. In this case, many features—for instance, the nature of the two phases that are separated by the transition—are independent of the microscopic details and can be determined in simplified models that are only characterized by a few properties, like the global and local symmetries, the dimensionality of the order parameter and the nature of the symmetry breaking pattern at the transition. In a finite-size system, long-distance global quantities have a nonanalytic dependence on the system size, which is also independent of the specific nature of the interactions and of the boundary conditions, which, however, may affect scaling functions and universal amplitudes, see, for example [1]. A second class of transitions are the first-order ones, characterized by the discontinuity of thermodynamic and global observables. From the point of view of phase behavior, discontinuous transitions are more interesting, as their phase behavior is more diverse. For instance, the nature of the coexisting phases crucially depends on the nature of the boundary conditions, even in the infinite-volume limit, see, for example [2]. Therefore, by simply varying the boundary interactions, one can generate a variety of different bulk behaviors.

In this work, we consider the one-dimensional quantum XY model in a transverse magnetic field [3–10], a paradigmatic integrable system, for which it is possible to obtain exact results for many ground-state properties, using its relation with a model of nonlocal free fermions. The Hamiltonian of an XY chain of length L is given by

$$H = -\frac{1}{2}\sum_{i=1}^{L-1}\left[(1+\gamma)\,\sigma_i^{(1)}\,\sigma_{i+1}^{(1)} + (1-\gamma)\,\sigma_i^{(2)}\,\sigma_{i+1}^{(2)}\right] - g\sum_{i=1}^{L}\sigma_i^{(3)}\,, \tag{1}$$

where $\sigma^{(i)}$ are the Pauli matrices. It is easy to verify that the spectrum is invariant under $g \to -g$, so we can set $g \geqslant 0$ without loss of generality. For periodic or open boundary conditions, the model is also invariant under $\gamma \to -\gamma$. However, this symmetry is broken by the boundary conditions we will use and, therefore, we will consider positive and negative values of γ. For $\gamma = \pm 1$, we obtain the simpler Ising chain, while for $\gamma = 0$, the Hamiltonian becomes that of the XX chain with an enlarged U(1) symmetry.

For $g = 1$ and any γ, the system undergoes a continuous quantum transition that separates a paramagnetic (disordered) phase ($g > 1$) from an ordered phase with a degenerate ground state ($g < 1$). The nature of the latter phase depends on the boundary conditions. For periodic and open boundary conditions, the phase diagram for $g < 1$ is well known, see, for example [11]. For $g^2 + \gamma^2 > 1$, there is an ordinary ferromagnetic phase: in the infinite-volume limit the ground state is doubly degenerate. This degeneracy is lifted in a finite volume, with a gap that behaves as e^{-aL}. On the other hand, for $g^2 + \gamma^2 < 1$, an oscillatory phase appears: the energy gap shows oscillating behavior as

J. Stat. Mech. (2025) 023101

a function of the system size, and correlation functions show oscillations as a function of the distance. The behavior for $g^2+\gamma^2=1$ is somewhat peculiar, as the ground-state wavefunction factorizes into a product of single spin states [12, 13].

If boundary fields are added, the phase behavior for $g<1$ becomes more complex. The analysis of [14–16] for the Ising chain ($\gamma=1$) shows that the addition of oppositely oriented longitudinal magnetic fields at the chain boundaries stabilizes a new phase, named the kink phase. In this phase there is no ferromagnetic order and the low-energy excitations are propagating kink states [17] of momentum of order $1/L$. The kink phase and the ferromagnetic phase are separated by a continuous transition, with a universal crossover behavior. Using the quantum-to-classical mapping, one can relate this transition to the wetting transition [18–21] that occurs in classical two-dimensional Ising systems in a strip geometry [22–32].

The finite-size behavior of the Ising and of the XY chain has been extensively studied [1, 14–16, 33–46]. In this work, we study the finite-size behavior of the gap in the presence of oppositely oriented boundary longitudinal fields (OBF), extending the results obtained in [15, 16] for the Ising chain to the XY model. By combining analytic and numerical methods, we obtain exact results for the large-size behavior of the low-energy excitations of the model which, in turn, allow us to determine the different possible phases for $g<1$.

The two phases that occur when periodic boundary conditions are used, the conventional ferromagnetic phase (we name it the magnetized (M) phase) and the oscillatory phase (named the magnetized-incommensurate (MI) phase) also occur in the presence of OBF. In both cases the gap decreases exponentially, with additional size oscillations in the MI phase. If the boundary fields are sufficiently strong, we find a kink (K) phase, as in the Ising chain [15], with delocalized excitations and a gap that decreases as $1/L^2$. Finally, we find a novel phase, that we name the kink-incommensurate (KI) phase, in which excitations are delocalized, so that the gap decreases as $1/L^2$, but which is also characterized by incommensurate oscillations, as the MI phase. We have also studied the behavior of the gap along the boundaries that separate the different phases. In particular, along the K-KI boundary, we find that the gap scales as L^{-4}, i.e. with a dynamical critical exponent $z=4$.

Finally, we discuss the crossover behavior that is observed when parameters are varied across a phase boundary. We have considered the crossover between the M and the K phase, obtaining the same behavior as observed in the Ising chain. As expected, the crossover across the M-K boundary is universal. We also discuss the behavior across the K-KI boundary. Also, in this case, we find a universal scaling regime. We determine the appropriate scaling variable and compute the scaling function for the energy gap.

The paper is organized as follows. In section 2, we introduce the one-dimensional quantum XY chain with boundary fields. In sections 3 and 4, we compute the low-energy spectrum by generalizing the approach of [16] and exploiting the equivalent quadratic fermionic formulation of the Hamiltonian [3, 7]. The different phases are discussed in the subsequent sections. In section 5, we sketch the phase diagram as a function of the model parameters and characterize the behavior of the low-energy excitations in the different phases. In section 6, we discuss the magnetized phases, and in section 7, the kink phase. In sections 8 and 9, we discuss the crossover behavior across the M-K

J. Stat. Mech. (2025) 023101

and K-KI boundaries. In section 10, we present our conclusions. Technical details are reported in the appendices.

2. Model and definitions

In this work, we focus on the low-energy spectrum of the XY model with Hamiltonian (1). It is important to observe that the model is ferromagnetic for any value of γ. For $|\gamma| \leqslant 1$, both hopping terms favor the alignment of the neighboring spins. For $|\gamma| > 1$, instead, the two terms have opposite signs, i.e. one is ferromagnetic and one is antiferromagnetic. The ferromagnetic interaction, however, is always the dominant one.

The XY chain undergoes a continuous transition at $g = 1$ [3, 4], separating a quantum ordered phase ($g < 1$) from a quantum paramagnetic phase ($g > 1$). In this paper, we investigate the effects of boundary magnetic fields aligned along the x axis. They give rise to an additional energy term

$$H_b = -\zeta_1 \sigma_1^{(1)} - \zeta_L \sigma_L^{(1)}, \tag{2}$$

which is added to Hamiltonian (1). In the following, we only consider the case of OBF, that correspond to

$$\zeta_1 = -\zeta_L. \tag{3}$$

We focus on the low-energy spectrum of the model. In particular, we will obtain exact finite-size results for the energy differences between the lowest states and the ground state

$$\Delta_n \equiv E_n - E_0, \tag{4}$$

(here, E_n are the energy eigenvalues ordered so that $E_0 \leqslant E_1 \leqslant E_2 \ldots$) and, in particular, for the finite-size gap $\Delta = E_1 - E_0$.

3. Jordan–Wigner representation and Hamiltonian diagonalization

To determine the spectrum of Hamiltonian (1), we use the technique introduced in [15]. We extend the model, considering two additional spins located in 0 and $L+1$ and the Hamiltonian

$$H_e = -\frac{1}{2}\sum_{i=1}^{L-1}\left[(1+\gamma)\,\sigma_i^{(1)}\sigma_{i+1}^{(1)} + (1-\gamma)\,\sigma_i^{(2)}\sigma_{i+1}^{(2)}\right] - J_0\,\sigma_0^{(1)}\sigma_1^{(1)} - J_L\,\sigma_L^{(1)}\sigma_{L+1}^{(1)} - g\sum_{i=1}^{L}\sigma_i^{(3)}. \tag{5}$$

This is the XY Hamiltonian with two different couplings on the boundary links and zero transverse field on the boundaries. To compute the spectrum of Hamiltonian (5),

J. Stat. Mech. (2025) 023101

we follow [15]. We first perform a Jordan–Wigner transformation, and then we perform a Bogoliubov transformation (see appendix A for details). The Hamiltonian takes the form

$$H_e = E_{gs} + \sum_{k=0}^{L+1} \mathcal{E}_k \eta_k^\dagger \eta_k, \tag{6}$$

with $0 \leqslant \mathcal{E}_0 \leqslant \mathcal{E}_1 \leqslant \ldots$, where η_k are canonical fermionic operators, and

$$E_{gs} = -\frac{1}{2} \sum_{k=0}^{L+1} \mathcal{E}_k. \tag{7}$$

The squared energies $\mathcal{E}_k^2$ of the fermionic modes are the eigenvalues of the matrix C given by

$$C = \begin{pmatrix} e & h & d & & & & & & \\ h & f & c & b & & & & & \\ d & c & a & c & b & & & & \\ 0 & b & c & a & c & b & & & \\ & & \ddots & \ddots & \ddots & \ddots & \ddots & & \vdots \\ & & & b & c & a & c & b & 0 \\ & & & & b & c & a & c & 0 \\ & & & & & b & c & l & 0 \\ & & & & \ldots & 0 & 0 & 0 & 0 \end{pmatrix} \tag{8}$$

with

$$\begin{aligned} a &= 2\left(1+\gamma^2\right) + 4g^2 \\ b &= 1-\gamma^2 \\ c &= 4g \\ d &= 2J_0\left(1-\gamma\right) \\ e &= 4J_0^2 \\ f &= 4g^2 + \left(1+\gamma\right)^2 \\ h &= 4J_0 g \\ l &= 4J_L^2 + 4g^2 + \left(1-\gamma\right)^2. \end{aligned} \tag{9}$$

The matrix C has a zero eigenvalue, $\mathcal{E}_0^2 = 0$, that is related to the double degeneracy of the spectrum of H_e (see appendix A for a more detailed discussion). To determine the non-zero eigenvalues, we consider the square matrix $\hat{C}$ of size $(L+1)\times(L+1)$ that is obtained from C by deleting the last column and the last row. The gap in the presence of OBF is expressed [15] in terms of the two lowest eigenvalues of $\hat{C}$, $\mathcal{E}_1^2$ and $\mathcal{E}_2^2$, computed by setting $J_0 = J_L = \zeta_1 = -\zeta_L$, as

$$\Delta_{\mathrm{OBF}} = \mathcal{E}_2 - \mathcal{E}_1. \tag{10}$$

J. Stat. Mech. (2025) 023101

4. Determination of the spectrum

To determine the spectrum of the matrix $\hat{C}$, we extend the results of [16, 46]. Reference [16] introduced a parametrization of the eigenvectors of the matrix $\hat{C}$ that is exact for the Ising chain ($\gamma = 1$). This parametrization was generalized in [46] to discuss the spectrum of the XY chain. Although it does not provide exact eigenvectors of $\hat{C}$ for finite values of L, [46] argued that the approximation becomes exact in the infinite-size limit, if the eigenvectors are localized (if the ground state is magnetized in the language we use in this paper). Here, we generalize the approach of [16], obtaining the exact eigenvectors ψ_L of $\hat{C}$ for any finite L. By definition, they satisfy the eigenvalue equations

$$\mathrm{Eq}_k = \sum_i \hat{C}_{ki}\psi_{L,i} - \mathcal{E}^2\psi_{L,k} = 0, \tag{11}$$

with $k, i = 1, \ldots, L+1$.

To determine ψ_L, we first note that a vector of components

$$\bar{\psi}_{L,1} = \frac{1+\gamma}{2J_0} A\,(-x) \quad \bar{\psi}_{L,k} = A(-x)^k \quad \text{for } k \geqslant 2, \tag{12}$$

(x and A are arbitrary complex numbers) satisfies equation (11) for any $k = 3, \ldots, L-1$, provided we identify $\mathcal{E}^2 = \varepsilon^2(x)$, where

$$\varepsilon^2(x) = \left(1-\gamma^2\right)\left(x + x^{-1}\right)^2 - 4g\left(x + x^{-1}\right) + 4\left(g^2+\gamma^2\right). \tag{13}$$

Equation (11) for the boundary components $k = 1, 2, L, L+1$ instead is not satisfied, and therefore this vector is not an eigenvector of $\hat{C}$. To obtain an eigenvector, we define ψ_L as a linear combination of vectors of the form reported above. The vector ψ_L depends on a few parameters that are fixed by requiring equation (11) to also hold on the boundaries, i.e. for $k = 1, 2, L, L+1$.

Specifically, as in [46], we consider two different complex numbers x_1 and x_2. Then, we parametrize the eigenvectors of $\hat{C}$ as[3]

$$\begin{aligned} \psi_{L,1} &= \frac{1+\gamma}{2J_0}\left(c_1 x_1^2 + c_2 x_2^2 + d_1 x_1^{3-L} + d_2 x_2^{3-L}\right), \\ \psi_{L,i} &= (-1)^{i-1}\left(c_1 x_1^{3-i} + c_2 x_2^{3-i} + d_1 x_1^{2-L+i} + d_2 x_2^{2-L+i}\right), \end{aligned} \tag{14}$$

where $i = 2, \ldots, L+1$. With the parametrization, equation (14), equations $\mathrm{Eq}_k = 0$ with $k = 3, \ldots, L-1$ are exactly satisfied for any c_1, c_2, d_1 and d_2, provided that $\mathcal{E}^2 = \varepsilon^2(x_1) = \varepsilon^2(x_2)$. If we require ψ_L to be an eigenvector of $\hat{C}$, equations $\mathrm{Eq}_k = 0$ for $k = 1, 2, L, L+1$ should also be satisfied. Explicitly, they can be written as:

[3] To make contact with equation (12), note that the terms with coefficient c_1 correspond to a vector $\bar{\psi}_L$ with $A = -c_1 x_1^3$ and $x = 1/x_1$, while those with coefficient d_1 correspond to a vector $\bar{\psi}_L$ with $A = -d_1 x_1^{2-L}$ and $x = x_1$.

J. Stat. Mech. (2025) 023101

$$\begin{aligned}
\mathrm{Eq}_1 &= c_1 E(x_1) F(x_1) + c_2 E(x_2) F(x_2) \\
&\quad + d_1 x_1^{5-L} E\left(x_1^{-1}\right) F\left(x_1^{-1}\right) + d_2 x_2^{5-L} E\left(x_2^{-1}\right) F\left(x_2^{-1}\right) = 0, \\
\mathrm{Eq}_2 &= c_1 E(x_1) + c_2 E(x_2) + d_1 x_1^{5-L} E\left(x_1^{-1}\right) + d_2 x_2^{5-L} E\left(x_2^{-1}\right) = 0, \\
\mathrm{Eq}_L &= \left(1-\gamma^2\right)\left(c_1 x_1^{1-L} + c_2 x_2^{1-L} + d_1 x_1^4 + d_2 x_2^4\right) = 0, \\
\mathrm{Eq}_{L+1} &= d_1 A(x_1) + d_2 A(x_2) + c_1 A\left(x_1^{-1}\right) x_1^{3-L} + c_2 A\left(x_2^{-1}\right) x_2^{3-L} = 0,
\end{aligned} \tag{15}$$

with

$$\begin{aligned}
A(x) &= x^2\left[(1+\gamma)^2 + x^2\left(1-\gamma^2\right) - 4gx - 4J_L^2\right], \\
E(x) &= x^3(1-\gamma)\left[1+\gamma-2gx^{-1}+(1-\gamma)x^{-2}\right], \\
F(x) &= -\frac{(\gamma+1)\left(-\gamma+2gx+(\gamma-1)x^2-1\right)+4J_0^2}{2(\gamma-1)J_0 x}.
\end{aligned} \tag{16}$$

Let us note that the second and the third equation in equation (15) are trivial for $\gamma = 1$, since in the transverse-field Ising chain there are only two nontrivial equations, see [16].

Equation (15) together with the constraint $\varepsilon^2(x_1) = \varepsilon^2(x_2)$ allow us to determine the parameters x_1 and x_2 and the coefficients c_1, c_2, d_1 and d_2 (up to a common multiplicative constant) that make ψ_L an eigenvector of $\hat{C}$.[4] Once these quantities are determined, the energies are obtained using $\mathcal{E}^2 = \varepsilon(x_1)^2$ or, equivalently, $\mathcal{E}^2 = \varepsilon(x_2)^2$.

Note that the parametrization is invariant under the exchange of x_1 and x_2, and under a second set of symmetries. If we define

$$c_1' = d_1 x_1^{5-L} \qquad d_1' = c_1 x_1^{5-L}, \tag{17}$$

we have

$$c_1 x_1^{3-i} + d_1 x_1^{2-L+i} = c_1'\left(\frac{1}{x_1}\right)^{3-i} + d_1'\left(\frac{1}{x_1}\right)^{2-L+i}, \tag{18}$$

which shows that the parametrization is invariant under $x_1 \to 1/x_1$. The same holds for the parameter x_2. The presence of these symmetries allows us to always choose x_1 and x_2 such that $|x_1| \geqslant 1$, $|x_2| \geqslant 1$, and $|x_1| \geqslant |x_2|$. Moreover, ψ_L is defined up to a multiplicative constant. Thus, we can arbitrarily set one of the parameters c_1, c_2, d_1 and d_2 equal to one or zero.

It is important to stress that the relevant parameters for the analysis of the spectrum are the two complex numbers x_1 and x_2. Indeed, each eigenvalue $\mathcal{E}^2$ is uniquely related with a pair x_1, x_2 of solutions of the equation $\mathcal{E}^2 = \varepsilon(x)^2$.[5] Since the parametrization is invariant under $x_i \to 1/x_i$ and under the exchange of x_1 and x_2, x_1 and x_2 can be identified with any pair of solutions that are not related by the inversion symmetry.

[4] This procedure allows us to obtain vectors ψ_L that are eigenvectors of $\hat{C}$ for finite L. In appendix B we prove that this approach provides all eigenvectors of $\hat{C}$.

[5] In some cases we will need to explicitly specify to which eigenvalue the values x_1 and x_2 correspond. As we label the eigenvalues of $\hat{C}$ with a positive integer n (the nth eigenvalue is $\mathcal{E}_n^2$), we refer to the corresponding values of x_1 and x_2 as $x_{1,n}$ and $x_{2,n}$. An analogous notation will be used for the coefficients that parametrize the large-L behavior of x_1 and x_2. Thus, if we define $x_2 \approx \exp(\mathrm{i}\theta_1/L)$, $\theta_{1,n}$ indicates the value of θ_1 for the nth eigenvalue of $\hat{C}$.

J. Stat. Mech. (2025) 023101

To make contact with the solution in the presence of periodic boundary conditions, see, for example [11], note that, if $x = e^{iq}$, the function $\varepsilon(x)$ can be rewritten as

$$\varepsilon\left(e^{iq}\right)^2 = 4\left[(g-\cos q)^2 + \gamma^2 \sin^2 q\right], \tag{19}$$

which is the dispersion relation between the momentum q and the energy for the XY model with periodic boundary conditions. Thus, in our parametrization, the eigenstates are linear combinations of two different excitations, whose momentum is encoded in the parameters x_1 and x_2. These excitations are delocalized if $|x_i| = 1$, localized in the opposite case.

In the following, we will study the phase diagram of the model for $J_0 > 0$. The case $J_0 = 0$ (open boundary conditions) can also be addressed with the same method, but requires *a priori* separate treatment, since our parametrization becomes singular in the limit $J_0 \to 0$, see equation (14). In practice, only the coefficients c_i and d_i are singular for $J_0 \to 0$. The parameters x_i are continuous and thus all the results for the phase diagram also apply for $J_0 = 0$, i.e. for open boundary conditions. We only consider the case $0 < g < 1$, in which the bulk behavior depends on the boundary conditions. Indeed, for $g > 1$, the system is paramagnetic and the gap is finite while, for $g = 1$, the behavior is independent of the microscopic details and thus the value of γ only affects nonuniversal constants and scaling corrections [1].

5. Numerical determination of the phase diagram

As we have already discussed, the parameters x_1 and x_2 satisfy $\varepsilon(x)^2 = \mathcal{E}^2$. Let us first discuss some general properties of the solutions of this equation, assuming that the eigenvalue $\mathcal{E}^2$ is known. First, if x is a solution, $1/x$ is also a solution. Moreover, if x is a complex solution, its complex conjugate $\bar{x}$ is also a solution. These two properties allow us to classify the solutions of the equation into four classes:

i) All solutions are real, with $|x| \neq 1$; they can be written as $x = p,\ q,\ 1/q,\ 1/p$, where p and q are real numbers satisfying $|p|, |q| > 1$.
ii) There are four complex solutions with $|x| \neq 1$. They can be parametrized as $x = pe^{i\phi}$, $pe^{-i\phi}$, $e^{i\phi}/p$, $e^{-i\phi}/p$, where p is a real positive number with $p > 1$.
iii) There are two real solutions with $|x| \neq 1$ and two complex solutions with $|x| = 1$. They can be parametrized as $x = p, 1/p, e^{i\phi}, e^{-i\phi}$, where p is a real number with $|p| > 1$.
iv) There are four complex solutions with $|x| = 1$ that can be parametrized as $(0 \leqslant \phi_1, \phi_2 \leqslant \pi)$ $x = e^{i\phi_1}, e^{i\phi_2}, e^{-i\phi_1}, e^{-i\phi_2}$.

The solutions x_i provide the two quantities x_1 and x_2 that we use to parametrize the eigenvectors of $\hat{C}$. The equations, as well as the parametrization of the eigenvectors, are invariant under $x_1 \to 1/x_1$, $x_2 \to 1/x_2$ and under the exchange of x_1 and x_2, and thus any pair of solutions that are not related by the inversion symmetry $(x \to 1/x)$ can be identified with x_1 and x_2. To unambiguously define the two parameters, we define

J. Stat. Mech. (2025) 023101

x_1 and x_2 such that $|x_1|, |x_2| \geqslant 1$ and $|x_1| \geqslant |x_2|$. More precisely, let us assume that the parameters p, q, ϕ, ϕ_1 and ϕ_2 that we have used above to parametrize the solutions satisfy $|p| > |q| > 1$, $0 \leqslant \phi, \phi_1, \phi_2 \leqslant \pi$, and $\phi_1 > \phi_2$. Then, we define:

Solutions i): $x_1 = p$, $x_2 = q$.
Solutions ii): $x_1 = p\mathrm{e}^{\mathrm{i}\phi}$, $x_2 = p\mathrm{e}^{-\mathrm{i}\phi}$.
Solutions iii): $x_1 = p$, $x_2 = \mathrm{e}^{\mathrm{i}\phi}$.
Solutions iv): $x_1 = \mathrm{e}^{\mathrm{i}\phi_1}$, $x_2 = \mathrm{e}^{\mathrm{i}\phi_2}$.

In the following, we will always assume that x_1 and x_2 have been determined as discussed here.

As a first step of our analysis, we perform a numerical study, with the purpose of determining x_1 and x_2 in the infinite-chain limit, for given model parameters g, γ and J_0. For this purpose, we determine the two lowest eigenvalues $\mathcal{E}_1^2$ and $\mathcal{E}_2^2$ of the matrix $\hat{C}$ for a given size L using a standard numerical algorithm and then we solve the equation $\varepsilon(x)^2 = \mathcal{E}_i^2$. This procedure allows us to compute $x_1(L)$ and $x_2(L)$ for the two eigenvalues. We repeat the procedure for several values of L (typically, L varies from 20 up to 100–300) and then we analyze the size behavior of the solutions. For some parameter values we observe a very fast convergence: within errors, the estimates of $\mathcal{E}_1$ and $\mathcal{E}_2$ are approximately the same and do not depend on L for $L \gtrsim 100$. In this case, we take the results for $L = 100$ as the infinite-chain estimates of x_1 and x_2. This type of behavior occurs when the parameters satisfy $|x_1| > 1$ and $|x_2| > 1$, i.e. when the solutions are of type (i) or (ii). For some other parameter values, instead, $\mathcal{E}_1$ and $\mathcal{E}_2$ show a significant size dependence. Size corrections apparently decay as an inverse power of L. Therefore, if $x_i(L)$ is real, it is extrapolated to $a_0 + a_1/L + a_2/L^2$. If $x_i(L)$ is complex, we separately extrapolate $|x_i(L)|$ and the corresponding phase to $a_0 + a_1/L + a_2/L^2$. As expected (for $g < 1$, the ground state is degenerate in the infinite-size limit), the extrapolated values for the two levels are approximately the same. This type of convergence occurs when the solutions are of type (iii) or (iv).

As an example, in figure 1 we report the infinite-length estimates of $|x_1|$ and $|x_2|$ as a function of g for different values of J_0 and γ. The boundaries between the different types of solutions have been obtained using the exact results presented in the following sections. In the upper left panel, solutions change from type (i) to type (iii) as g increases, while in the lower panels, we go from type (iv) to type (iii). In the upper right panel, as g increases, we observe the transitions (ii)$\rightarrow$ (i) $\rightarrow$ (iii).

The analysis of the size behavior of the eigenvalues $\mathcal{E}_i$ suggests that there is a strict relation between the nature of the solutions of the equation $\varepsilon(x)^2 = \mathcal{E}_i^2$ and the phase behavior of the model. This is even more evident from the analysis of the gap, which shows that the parameter space J_0, γ, g $(0 \leqslant g < 1)$ can be divided into four phases. In each phase, the parameters x_1 and x_2 belong to one of the four classes discussed above.

If, for given Hamiltonian parameters, x_1 and x_2 are both real (solutions of type (i)), we find that the gap $\Delta = E_1 - E_0$ decreases exponentially with the chain length. This is the behavior expected at a magnetic first-order transition: thus, solutions of type (i) characterize what we name the magnetized (M) phase. If the values of x_1 and x_2

J. Stat. Mech. (2025) 023101

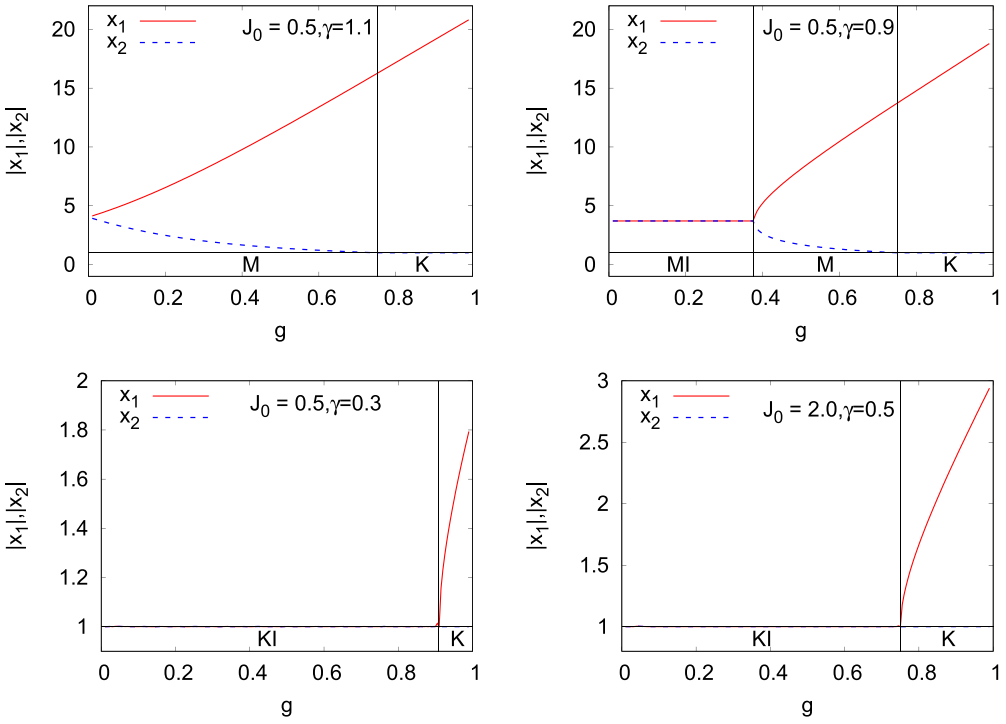

Figure 1. Plots of $|x_1|$ and $|x_2|$ as a function of g, for given J_0 and γ. (a) (Top left) Here, x_1 and x_2 are both real (M phase, type (i) solution) for $g \lesssim 0.755$, while x_1 is real and x_2 is complex (K phase, type (iii) solution) in the opposite case. (b) (Top right) Here, x_1 and x_2 are both complex (MI phase, type (ii) solution) with $|x_1| = |x_2| > 1$ up to $g \approx 0.377$; then, they become real (M phase, type (i) solution) up to $g \approx 0.752$. For larger values of g, x_1 is real and x_2 is complex (K phase, type (iii) solutions). (c) (Bottom) In both cases for small g, we have $|x_1| = |x_2| = 1$ (KI phase, type (iv) solution). Then, x_1 becomes real, while x_2 is complex (K phase, type (iii) solution); the transition occurs for $g \approx 0.908$ (left) and $g = 0.75$ (right).

for given Hamiltonian parameters are of type (ii), the system is also in a magnetized phase, since size corrections decay exponentially with L. However, in this case, the gap behaves as $\Delta = f(L)\mathrm{e}^{-mL}$, where $f(L)$ is an oscillatory bounded function, whose oscillations are not commensurate with the chain size. We will name this phase the MI phase. The size behavior changes at phase points where $|x_2| = 1$, i.e. if x_1 and x_2 are solutions of type (iii) and (iv). If x_1 is real (solutions of type (iii)), the gap scales as $1/L^2$: the corresponding phase will be named the kink (K) phase. When x_1 is also complex with $|x_1| = 1$ (the solution is of type (iv)), there are additional oscillations and the gap decreases as $\Delta = f(L)/L^2$ for large L, where $f(L)$ is an incommensurate oscillatory bounded function. This phase will be named the KI phase.

In figures 2–4, we anticipate the phase diagrams obtained from the analysis. For fixed values of J_0, there are three possible different regimes that correspond to $0 < J_0 < 1$ and $\gamma > 0$, to $J_0 \geqslant 1$ and $\gamma > 0$, and to $\gamma < 0$—in this last case the value of J_0 is irrelevant. In the first case, we observe all four possible phases (see the panels for $J_0 = 0.5$ and $J_0 = 0.9$ in figure 2). For small values of γ, the system is in the KI phase for small g

J. Stat. Mech. (2025) 023101

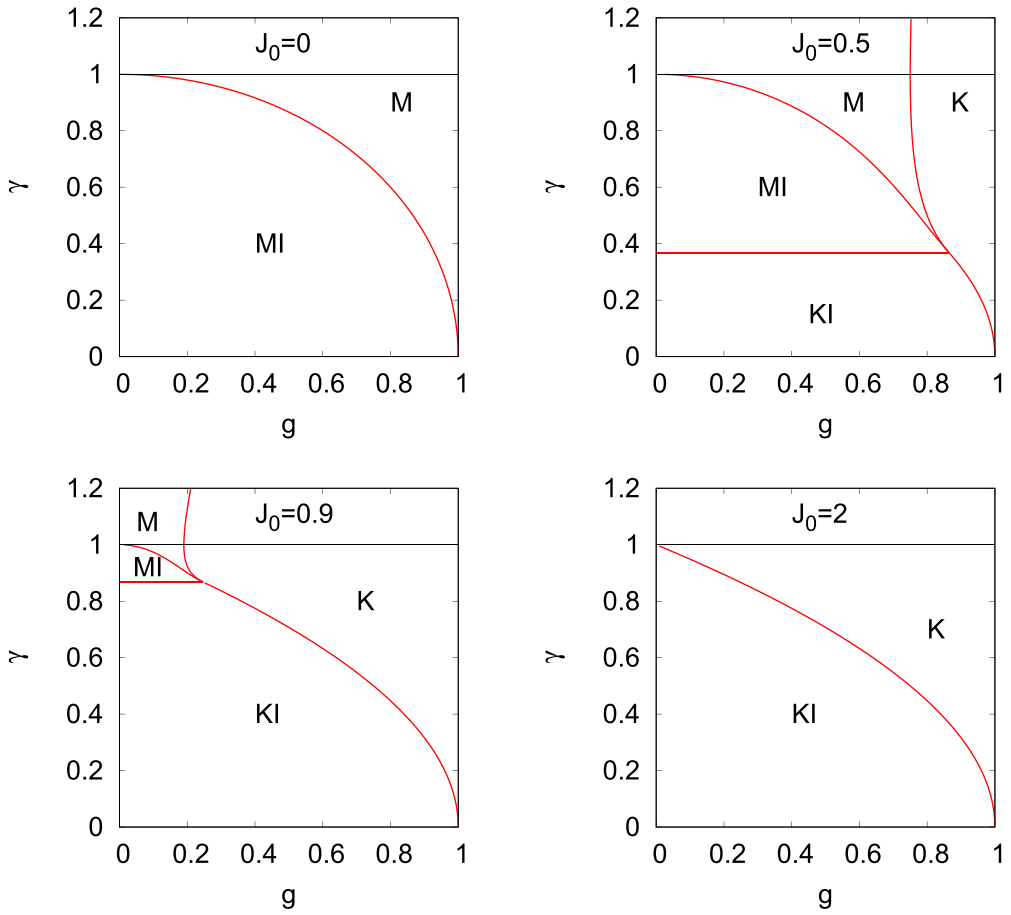

Figure 2. Phase diagrams in the $g-\gamma$ plane for fixed values of J_0 and positive values of γ: behavior for $J_0=0$ (top left), $J_0=0.5$ (top right), $J_0=0.9$ (bottom left) and $J_0=2$ (bottom right).

and in the K phase for g close to 1. As γ increases, the KI phase is replaced by the MI (for small g and only up to $\gamma=1$) and by the M (intermediate values of g) phase. The behavior changes as J_0 increases. Indeed, the M and the MI phases shrink and disappear for $J_0=1$. For larger values of J_0, the phase diagram is independent of J_0, with two phases, the KI phase (in the region $\gamma<1$) and the K phase: see the panel for $J_0=2$ in figure 2. In figure 3, we report the phase diagrams for two fixed values of γ. For $\gamma=2$, the behavior is analogous to that observed in the Ising chain, with a magnetized phase for small boundary fields and a kink phase for large values. For $\gamma=0.6$, all four different phases appear.

The behavior for $\gamma<0$ is independent of J_0, see figure 4, and is the same as in the case of periodic boundary conditions: the boundary between the MI and the M phase satisfies the equation $g^2+\gamma^2=1$. The same phase behavior is observed for $J_0=0$ (open boundary conditions). This result is quite obvious for the Ising chain with $\gamma=-1$. Indeed, for this value of γ, the system orders ferromagnetically in the y direction, irrespective of the boundary fields that instead point in the x direction.

J. Stat. Mech. (2025) 023101

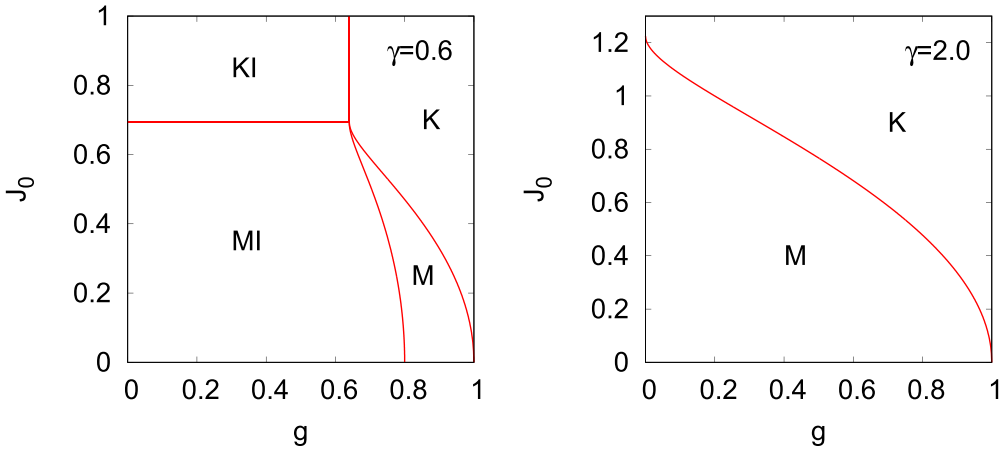

Figure 3. Phase diagrams in the $g - J_0$ plane for fixed values of γ: behavior for $\gamma = 0.6$ (left) and for $\gamma = 2.0$ (right).

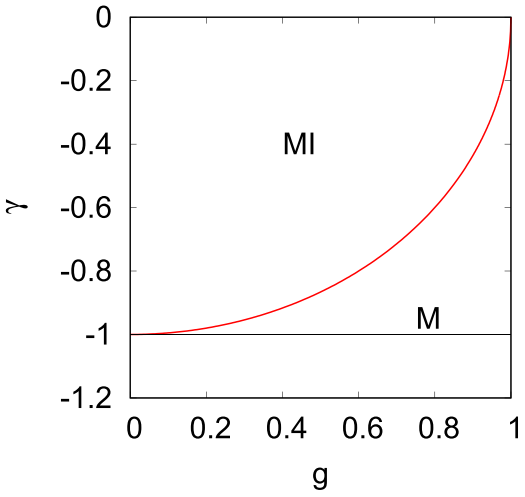

Figure 4. The phase diagram in the $g - \gamma$ plane for $\gamma < 0$. The phase diagram does not depend on J_0.

6. The magnetized phases

We now wish to characterize the magnetized phases. In the infinite-size limit we expect two degenerate solutions of the eigenvalue equation. No degeneracy is present for finite L, and therefore we expect two low-lying states with an exponentially small gap. In section 6.1, we determine the values of the parameters x_1 and x_2 that correspond to the two degenerate ground-state eigenvectors (details are given in appendix C), while in section 6.2, we determine for which values of the parameters the system is in the magnetized phases (M and MI phases, as discussed in section 5).

J. Stat. Mech. (2025) 023101

6.1. Determination of the parameters x_1 and x_2

In this section, we compute x_1 and x_2 for the ground state in the infinite-chain limit. As discussed in section 5, in the magnetized phases, $|x_1|$ and $|x_2|$ are both larger than 1. Therefore, for large system sizes, the quantities x_1^{-L} and x_2^{-L} are exponentially small and thus the leading behavior is obtained by neglecting these exponential terms. Equation (15) is analyzed in appendix C. For $\gamma > 0$, x_1 and x_2 are solutions of

$$x_1 x_2 = \frac{(1+\gamma)^2 - 4J_0^2}{1-\gamma^2}\,, \tag{20}$$

$$x_1 + x_2 = \frac{2g\left[(1+\gamma)^2 - 4J_0^2\right]}{(1-\gamma^2)\,(1+\gamma-2J_0^2)}. \tag{21}$$

On the other hand, for $\gamma < 0$, x_1 and x_2 both satisfy $f_1(x_i) f_1(1/x_i) = 0$, where the function $f_1(x)$ is defined as

$$f_1(x) = (1+\gamma)\,x^2 - 2gx + (1-\gamma) = 0. \tag{22}$$

If the solutions are both real and larger than 1 in absolute value, the system is in the M phase for the given set of parameters. If they are complex conjugate with $|x_1| = |x_2| > 1$, the system is in the MI phase.

It is important to note that, for each set of Hamiltonian parameters, we obtain two independent eigenvectors, as expected in a magnetized phase. In a finite volume the degeneracy is lifted. The splitting of the two degenerate levels should be due to the terms of order x_1^{-L} and x_2^{-L} that are neglected in the computation of the infinite-size behavior. Since $|x_2| \leqslant |x_1|$, the gap should scale as $|x_2|^{-L}$, with incommensurate oscillations if x_2 is complex.

In figure 5, we show the rescaled gap for some points that correspond to the four different phases. The results for the MI and M phases (see the lower panels) are rescaled by $|x_2|^L$ and x_2^L, respectively, where x_2 has been determined using equations (20) and (21). In the M case, $x_2^L \Delta(L)$ is apparently independent of L for $L \geqslant 20$, indicating that $\Delta(L) \approx a x_2^{-L}$ with negligible size corrections (they are expected to be of the order x_2^{2L} and x_1^L). In the MI case, the rescaled data are constant on average, but show oscillatory behavior: apparently, we have $|x_2|^L \Delta(L) \approx f(L)$, where $f(L)$ is a bounded oscillating function, so that $\Delta(L) \approx f(L)|x_2|^{-L}$.

Let us note that, in the M case, x_1 and x_2 should be both real and their absolute value should be larger than 1. This condition does not exclude that one or both of them is negative, smaller than -1. Numerically, we have found that x_2 is always positive, excluding the possibility of oscillations of the gap with the parity of the size: indeed, if $x_2 < -1$, we would have $\Delta(L) \approx a(-1)^L |x_2|^{-L}$. The absence of even–odd oscillations is expected as the model is ferromagnetic. Instead, x_1 is positive or negative, depending on γ: x_1 is positive for $|\gamma| < 1$ and negative in the opposite case. This last result can be explained by noting that, for $|\gamma| > 1$, the Hamiltonian is the sum of a ferromagnetic dominant hopping term and of an antiferromagnetic subdominant hopping term. Apparently, the latter term induces subdominant even–odd oscillations that decrease as $(-1)^L |x_1|^L$.

J. Stat. Mech. (2025) 023101

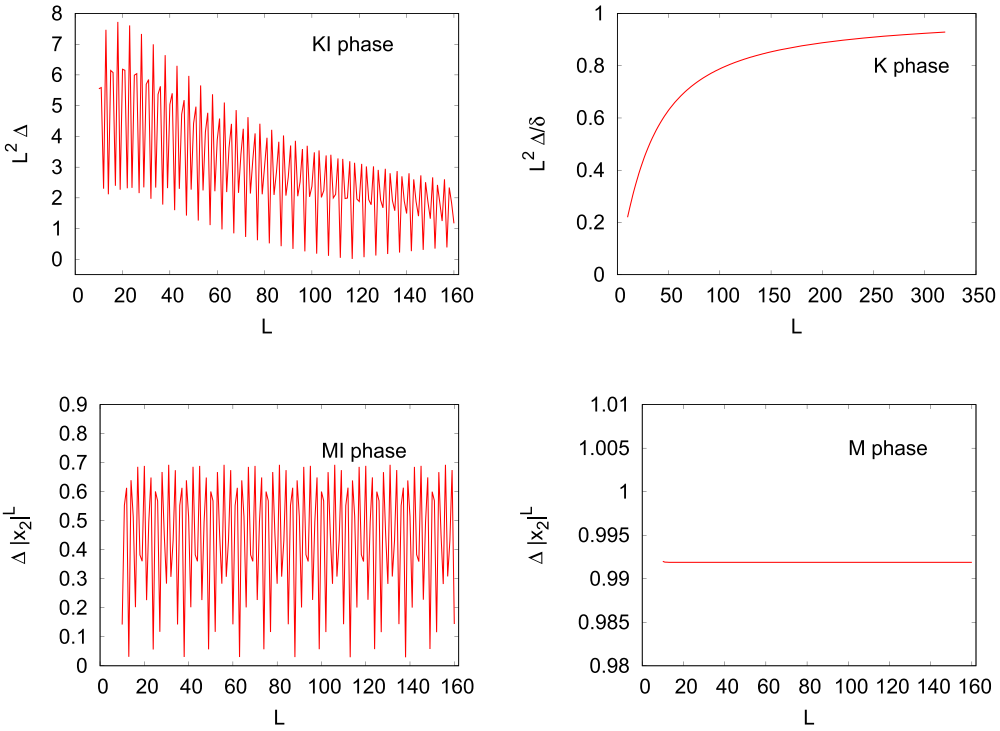

Figure 5. The rescaled gap for different sizes in the four phases. Top left: $g = 0.3$, $\gamma = 0.2$ (KI phase); top right: $g = 0.9$, $\gamma = 0.6$ (K phase); bottom left: $g = 0.3$, $\gamma = 0.6$ (MI phase); bottom right: $g = 0.3$, $\gamma = 1.2$ (M phase). In all cases $J_0 = 0.5$. The gap Δ has been determined numerically for several values of L, diagonalizing the matrix $\hat{C}$. We use the exact results for x_2 and δ. We have (see equations (20) and (21)) $|x_2| = 1.5612495$ for $g = 0.3$, $\gamma = 0.6$ (MI phase), $x_2 = 1.7914396$ for $g = 0.3$, $\gamma = 1.2$ (M phase), while, for $g = 0.9$ and $\gamma = 0.6$ (K phase), the gap behaves as δ/L^2 with $\delta = 76.9829$ (see equation (34)).

Finally, let us discuss the limits $\gamma \to \pm 1$, in which the XY chain becomes the simpler Ising chain. For $\gamma \to 1$, we have

$$x_1 \approx \frac{2g}{1-\gamma} \qquad x_2 = \frac{1-J_0^2}{g}. \tag{23}$$

As expected, x_1 and x_2 are real for γ close to 1, in agreement with the Ising results: no MI phase is observed in the Ising chain. Moreover, x_1 diverges as $\gamma \to 1$, in agreement with the fact that the Ising solution can be parametrized in terms of a single variable x, see [16]. The result for x_2 is in agreement with the results for the gap obtained in [15].

For $\gamma \to -1$, we instead obtain

$$x_1 \approx \frac{2g}{1+\gamma} \qquad x_2 = \frac{1}{g}. \tag{24}$$

As before, x_1 diverges on the Ising line. Here, x_2 is independent of J_0, and therefore the gap scales as for open boundary conditions ($J_0 = 0$).

J. Stat. Mech. (2025) 023101

6.2. Boundaries of the magnetized phases

We are now in the position to discuss the boundaries of the magnetized phases. We first discuss the behavior for $\gamma \geqslant 0$. In this case, the values of x_1 and x_2 are determined using equations (20) and (21). Let us first determine the boundary between the M and the MI phase. Since, in the MI phase, x_1 and x_2 are complex numbers satisfying $|x_1| = |x_2|$, while in the M phase they are real, on the boundary, x_1 and x_2 should be real satisfying $x_1 = \pm x_2$. As we have discussed above, the MI phase lies in the region $J_0 < 1$ and $\gamma < 1$. In this range of parameters, both x_1 and x_2 are positive and therefore the boundary is defined by $x_1 = x_2$. If we set $x_1 = x_2$ in equations (20) and (21) and solve for g (assuming $J_0 < 1$ and $\gamma < 1$), we obtain

$$g_{\mathrm{M/MI}} = \left(1 + \gamma - 2J_0^2\right) \sqrt{\frac{1-\gamma^2}{(1+\gamma)^2 - 4J_0^2}}\,. \tag{25}$$

At the boundary we have

$$x_{1,\mathrm{M/MI}} = x_{2,\mathrm{M/MI}} = \sqrt{\frac{(1+\gamma)^2 - 4J_0^2}{1-\gamma^2}}. \tag{26}$$

Since $J_0 < 1$, $g_{\mathrm{M/MI}}$ decreases as γ increases. Moreover, we have $g_{\mathrm{M/MI}} = 0$ for $\gamma = 1$. Note that we have $g_{\mathrm{M/MI}} = \sqrt{1-\gamma^2}$ for $J_0 = 0$, which is the result that also holds for periodic boundary conditions.

To derive the boundary between the KI phase and the MI phase, let us note that $x_1 = p\mathrm{e}^{\mathrm{i}\phi}$ and $x_2 = p\mathrm{e}^{-\mathrm{i}\phi}$ in the MI phase, and $x_1 = \mathrm{e}^{\mathrm{i}\phi_1}$ and $x_2 = \mathrm{e}^{\mathrm{i}\phi_2}$ in the KI phase. Thus, as we move in the MI phase toward the boundary, the parameter p converges to $p = 1$. Therefore, the boundary is characterized by the condition $x_1 x_2 = 1$. Equation (20) then gives

$$\gamma_{\mathrm{KI/MI}} = \frac{1}{2}\left(\sqrt{1 + 8J_0^2} - 1\right), \tag{27}$$

which is independent of g. Note that $\gamma_{\mathrm{KI/MI}}$ increases with increasing J_0 and that $\gamma_{\mathrm{KI/MI}} = 0, 1$ for $J_0 = 0, 1$, respectively. Moreover, $x_{1,\mathrm{M/MI}} = x_{2,\mathrm{M/MI}}$ is larger than 1 only for $\gamma > \gamma_{\mathrm{KI/MI}}$, so that the MI phase lies in the region $\gamma > \gamma_{\mathrm{KI/MI}}$ (see the phase diagrams for $J_0 = 0.5$ and 0.9 in figure 2).

Let us finally determine the boundary between the K phase ($x_1 > 1$ and $|x_2| = 1$) and the M phase ($|x_1|, |x_2| > 1$), which only exists for $J_0 < 1$: see the plots shown in figure 2. As we have already discussed, in the M phase x_2 is always positive and, therefore, the boundary is defined by the condition $x_2 = 1$. Substituting $x_2 = 1$ in equations (20) and (21), we obtain

$$g_{\mathrm{K/M}} = \frac{\left(1 + \gamma - 2J_0^2\right)^2}{(1+\gamma)^2 - 4J_0^2}, \tag{28}$$

J. Stat. Mech. (2025) 023101

with

$$x_{1,\mathrm{K/M}} = \frac{(1+\gamma)^2 - 4J_0^2}{1-\gamma^2}. \tag{29}$$

For $\gamma = 1$, we obtain $g_{\mathrm{K/M}} = 1 - J_0^2$, in agreement with the results of [15]. For $J_0 < 1$, the two conditions, (i) $g_{\mathrm{K/M}}$ is real and lies in $[0,1]$, and (ii) $x_{1,\mathrm{K/M}} > 1$, are satisfied only for $\gamma > \gamma_{\mathrm{KI/MI}}$. The boundary therefore lies in the region $\gamma > \gamma_{\mathrm{KI/MI}}$. Finally, let us note that, for fixed $J_0 < 1$, $g_{\mathrm{K/M}}$ decreases with increasing γ, reaches its minimum at $\gamma = 1$, and then increases, converging to 1 for $\gamma \to \infty$ (see the phase diagrams for $J_0 = 0.5$ and $J_0 = 0.9$ in figure 2). Correspondingly, $x_{1,\mathrm{K/M}}$ is an increasing positive function of γ for $\gamma < 1$, while it is a decreasing negative function of γ for $\gamma > 1$.

The three boundaries meet along a multicritical (MC) line characterized by the condition $x_1 = x_2 = 1$. We obtain

$$\gamma_{\mathrm{MC}} = \gamma_{\mathrm{KI/MI}} \qquad g_{\mathrm{MC}} = \frac{1}{2}\left(\sqrt{1+8J_0^2} + 1 - 4J_0^2\right) = 1 - \gamma_{\mathrm{MC}}^2. \tag{30}$$

The MC line only exists for $J_0 < 1$—for $J_0 > 1$ we indeed obtain $g_{\mathrm{MC}} < 0$—as the KI and MI phases. Note that g_{MC} is a decreasing function of J_0, satisfying $g_{\mathrm{MC}} = 1, 0$ for $J_0 = 0$ and 1.

The behavior for $\gamma < 0$ is much simpler. In this case, x_1 and x_2 are solutions of $f_1(x_1) = f_1(x_2) = 0$. They satisfy $|x_1| > 1$ and $|x_2| > 1$, and therefore there are only the M and the MI phases. For $\gamma \leqslant -1$, all points belong to the M phase, while, for $-1 < \gamma < 0$, systems with $g < \hat{g}_{\mathrm{M/MI}}$ are in the MI phase and systems with $g > \hat{g}_{\mathrm{M/MI}}$ are in the M phase. The boundary is specified by

$$\hat{g}_{\mathrm{M/MI}} = \sqrt{1-\gamma^2} \qquad x_{1,\mathrm{M/MI}} = x_{2,\mathrm{M/MI}} = \frac{g}{1+\gamma}. \tag{31}$$

The corresponding phase diagram is reported in figure 4.

It is interesting to compare our results with the expressions reported in [46]. They used an approximate ansatz to solve the eigenvalue equations, which is correct, in the infinite-chain limit, only in the magnetized phases. This approximation allowed them to correctly identify the boundary between the M phase and the MI phase, equation (25), as well as the position of the MC line, equation (30).

7. The kink phase

The kink phase has been extensively discussed in [15] for the Ising case $\gamma = 1$. For a finite chain of length L, the energies $\mathcal{E}_n$ of the lowest levels (the 'kink' states) are proportional to n^2/L^2 and, thus, in the infinite-length limit, there is an infinite number of degenerate states. As we shall see, the same result holds for the XY model.

In the kink phase, the relevant solutions are those of type (iii), i.e. x_1 is real and larger than 1 in absolute value, and x_2 is a complex number that satisfies $|x_2| = 1$ and that can therefore be written as $x_2 = \mathrm{e}^{\mathrm{i}\phi}$. A detailed analysis of the equations in equation (15)

is reported in appendix D. It turns out that if we only consider the low-lying energy states, we have, for large L

$$x_1 = x_{10} + O\left(L^{-2}\right) \qquad \phi = \frac{\theta_1}{L} + O\left(L^{-2}\right), \tag{32}$$

where

$$x_1 = x_{10} \equiv \frac{1}{1-\gamma^2}\left[2\sqrt{g(\gamma^2+g-1)} + \gamma^2 + 2g - 1\right]. \tag{33}$$

The phase θ_1 depends on the eigenvalue. For the nth level of the matrix $\hat{C}$ we have $\theta_{1,n} = n\pi$. Thus, the low-energy eigenvectors of $\hat{C}$ are superpositions of a 'localized' excitation (the contribution depending on x_1) and of a delocalized excitation of momentum $q = \phi = n\pi/L$, as for $\gamma = 1$.

Since the lowest-lying state corresponds to $x_{2,1} = \mathrm{e}^{\mathrm{i}\pi/L}$, while the first excited state corresponds to $x_{2,2} = \mathrm{e}^{2\mathrm{i}\pi/L}$ (with corrections of order $1/L^2$), the gap in the K phase is

$$\Delta = \varepsilon\left(x_{2,2}\right) - \varepsilon\left(x_{2,1}\right) = \frac{3\pi^2\left(\gamma^2+g-1\right)}{1-g}\frac{1}{L^2} + O\left(L^{-3}\right). \tag{34}$$

If we set $\gamma = 1$, we re-obtain the Ising-chain result of [15]. A numerical check of the validity of equation (34) is provided in figure 5. For $g = 0.9$, $\gamma = 0.6$ and $J_0 = 0.5$, we determine $\Delta(L)$ by numerically diagonalizing the matrix $\hat{C}$. Then, we report $\Delta(L)L^2/\delta$, where δ/L^2 is the expected leading behavior computed using equation (34). The ratio converges to 1 as L increases, confirming the correctness of equation (34).

In the K phase, the parameter x_1 should be real, which is only true for $g > 1-\gamma^2$. Since $x_{10} = 1$ for $g = 1-\gamma^2$, this condition characterizes the boundary between the K phase and the KI phase, i.e. the K-KI boundary is given by

$$g_{\mathrm{K/KI}} = 1 - \gamma^2. \tag{35}$$

This surface lies in the region $\gamma < 1$ and also ends at the MC line, equation (30), see, for example, the phase diagrams for $J_0 = 0.5$ and 0.9 in figure 2.

The K-KI boundary can also be determined by analyzing the minima of the dispersion relation, equation (19), which should apply both in the K and the KI phase as the low-energy behavior is associated with propagating excitations of *real* momentum q. In the K phase, $g > g_{\mathrm{K/KI}}$, $\varepsilon(\mathrm{e}^{\mathrm{i}q})$ has a minimum for $q = 0$, in agreement with the idea that the low-energy excitations are kink states of momentum $q \sim 1/L$. On the other hand, in the KI phase, the low-energy behavior is associated with propagating excitations of momenta $q = \pm q^*$ with $\cos q^* = g/(1-\gamma^2)$. References [47, 48] used these arguments to discuss the phase behavior of an antiferromagnetic XY model with frustrated boundary conditions. They found two different phases for $g > g_{\mathrm{K/KI}}$ and $g < g_{\mathrm{K/KI}}$ that we can identify with the K and KI phases that are present in the ferromagnetic case with OBF.

J. Stat. Mech. (2025) 023101

8. The boundary between the K and the M phases

8.1. Behavior along the boundary

Let us now determine the gap on the boundary between the M phase and the K phase. Equations (32) and (33) also hold on the boundary, with $x_{10} = x_{1,\mathrm{K/M}}$. Moreover, also in this case, the phases θ_1 are integer multiples of π, i.e. $\theta_1 = k\pi$. However, while inside the K phase only positive values of k are allowed, on the boundary, the value of x_2 corresponding to the state with energy $\mathcal{E}_1$ (the lowest eigenvalue) is $x_2 = 1$ with exponential corrections, which implies $\theta_1 = 0$. Therefore, on the boundary, we have $\theta_{1,n} = (n-1)\pi$ for the nth eigenvalue. This different behavior for points inside the K phase and on the M-K boundary is not surprising, as the same occurs in the Ising chain (for this model, analytic proof is given in [15]). Correspondingly, we obtain, for the gap $\Delta = \varepsilon(x_{2,1}) - \varepsilon(x_{2,0})$:

$$\Delta = \frac{\pi^2\left(\gamma^2+g-1\right)}{1-g}\frac{1}{L^2} + O\left(L^{-3}\right), \tag{36}$$

in full agreement with the Ising chain results [15].

8.2. Crossover behavior across the M-K boundary

References [14, 15] showed the presence of universal crossover behavior across the boundary between the M and the K phase. We will now show that the same behavior occurs for generic values of γ. We work with g and γ fixed, as in [15], and vary J_0 close to the boundary point

$$J_{0c} = \sqrt{\frac{1}{2}\left(\gamma - g + 1 - s\right)} \qquad s = \sqrt{g\left(\gamma^2+g-1\right)}, \tag{37}$$

which is obtained by inverting equation (25).

We parametrize the crossover in terms of the scaling variable [14, 15]

$$\zeta_s = RL\left(J_0 - J_{0c}\right), \tag{38}$$

where R is a nonuniversal parameter that will be determined below. In terms of this variable, in the large-L limit, we expect the scaling behavior

$$\frac{\Delta\left(J_0\right)}{\Delta\left(J_{0c}\right)} = f_\Delta\left(\zeta_s\right). \tag{39}$$

The constant R can be fixed so that $f_\Delta(\zeta_s)$ is universal, i.e. it is the same on the whole M-K boundary. In particular, we choose R to obtain the same scaling curves determined in [15]. The details of the calculation are reported in appendix E. We find

$$R = \frac{4gJ_{0c}}{\left(g+s\right)^2} \qquad s = \sqrt{g\left(\gamma^2+g-1\right)}. \tag{40}$$

J. Stat. Mech. (2025) 023101

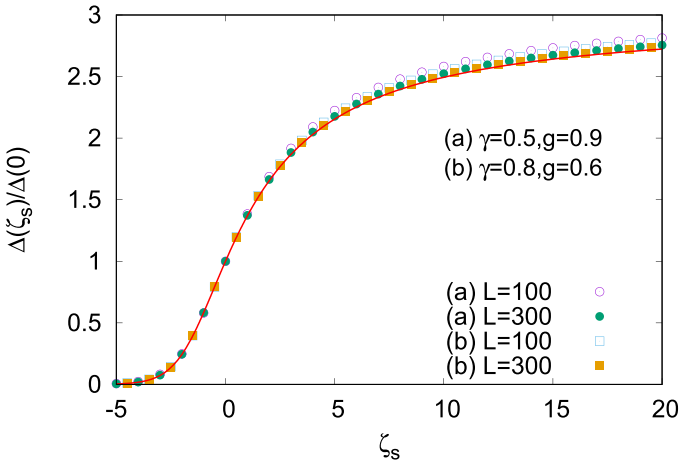

Figure 6. The ratio $\Delta(J_0)/\Delta(J_{0c})$ as a function of $\zeta_s = RL(J_0 - J_{0c})$ for two distinct points belonging to the M-K boundary. We used: (a) $J_{0c} = 0.341010$, $R = 0.764235$ for $\gamma = 0.5$ and $g = 0.9$; (b) $J_{0c} = 0.640518$, $R = 1.60235$ for $\gamma = 0.8$ and $g = 0.6$. The gap $\Delta(J_0)$ has been obtained by a numerical diagonalization of the matrix $\hat{C}$ for two different values of L. The continuous line is the universal scaling curve $f_\Delta(\zeta_s)$ computed in [15].

We can compare this expression with the Ising results obtained in [15]. For $\gamma = 1$, the boundary occurs at $J_{0c} = \sqrt{1-g}$. Correspondingly, we find $R = J_{0c}/g$, in agreement with [15].

To verify the previous calculations, in figure 6 we show the ratio $\Delta(J_0)/\Delta(J_{0c})$ for two different values of L and two different points belonging to the M-K boundary (the gap is obtained by a direct diagonalization of the matrix $\hat{C}$). Using the value of R reported in equation (40), as L increases, the data approach the universal curve derived in [15], confirming the universality of the scaling behavior.

9. The boundary between the K and the KI phases

9.1. Behavior along the boundary

We now discuss the behavior along the K-KI boundary, which is defined by the relation $g = 1 - \gamma^2$, see equation (35), with $\gamma > 0$. In the infinite-chain limit we have $x_1 = |x_2| = 1$ for the ground state. To proceed further, we need to determine the finite-size corrections to the previous relation. We have first performed a finite-size numerical analysis, finding that x_1 is real and larger than 1 for finite values of L, while x_2 is a phase that converges to 1 as L increases. Thus, for large values of L we can write

$$x_1 = 1 + \frac{x_{11}}{L} + O\left(L^{-2}\right) \qquad x_2 = 1 + \frac{i\,\theta_1}{L} + O\left(L^{-2}\right), \tag{41}$$

with x_{11} and θ_1 strictly positive. Inserting these expansions in the equation $\varepsilon(x_1)^2 = \varepsilon(x_2)^2$, we find $x_{11} = \theta_1$. To compute θ_1, we proceed as before, keeping both x_1^{-L} and

x_2^{-L}, as both quantities have a finite limit as $L \to \infty$. We consider equation (15), setting $c_2 = 1$. We eliminate c_1, d_1 and d_2, obtaining a single equation for θ_1, which is then expanded in powers of $1/L$. The leading term vanishes. Requiring the next-to-leading term to vanish, we obtain the relation

$$\cos\theta_1 \cosh\theta_1 = 1. \tag{42}$$

This relation, which is the same for all points that belong to the K-KI boundary, allows us to compute θ_1. There is a trivial solution $\theta_1 = 0$ and an infinite number of positive solutions that we indicate with $\bar{\theta}_{1,k}$, $k \geqslant 1$. The smallest positive solution $\bar{\theta}_{1,1}$ is

$$\bar{\theta}_{1,1} = 4.73004\ldots \tag{43}$$

Solutions $\bar{\theta}_{1,n} > \bar{\theta}_{1,1}$, $n = 2, 3\ldots$, can be accurately determined using

$$\bar{\theta}_{1,n} = k_n + \frac{(-1)^n}{\cosh k_n} \qquad k_n = \frac{\pi}{2}(2n+1). \tag{44}$$

In particular, $\bar{\theta}_{1,2} = 7.8532\ldots$. To understand the relation between the solutions $\bar{\theta}_{1,k}$ and the large-L behavior of x_1 and x_2 for the low-energy levels of $\hat{C}$, we have performed a detailed numerical analysis, computing $x_1(L)$ and $x_2(L)$, as described in section 5. We find $x_{2,n} = 1 + i\bar{\theta}_{1,n}/L$ for the nth eigenvalue of $\hat{C}$, i.e. the nth eigenvalue correction term $\theta_{1,n}$ is equal to $\bar{\theta}_{1,n}$. In particular, $\bar{\theta}_{1,1}$ and $\bar{\theta}_{1,2}$ refer to the ground state and to the first excited state, respectively. Given that $\theta_{1,n} = \bar{\theta}_{1,n}$, in the following we will label the solutions of equation (42) simply with $\theta_{1,n}$.

We can finally compute the gap. Since

$$\varepsilon(x_1)^2 \approx 4\gamma^4 + \left(1-\gamma^2\right)\theta_1^4 \frac{1}{L^4} \tag{45}$$

for large values of L, we obtain

$$\Delta_{\mathrm{K/KI}} = \frac{1-\gamma^2}{4\gamma^2}\left(\theta_{1,2}^4 - \theta_{1,1}^4\right)\frac{1}{L^4}. \tag{46}$$

While in the K and KI phases the gap decreases as L^{-2}, at the boundary between the two phases, the gap decreases faster, as L^{-4}: the dynamic exponent z is equal to 4.

To verify the predicted behavior, equation (46), we have considered points on the K-KI boundary and numerically computed the gap $\Delta(L)$ for different sizes (we determine it via a direct diagonalization of the matrix $\hat{C}$). As expected, the ratio $\Delta(L)/\Delta_{\mathrm{K/KI}}$ approaches 1 as L increases (numerically we find $1/L$ corrections), see figure 7.

Critical behavior with $z = 4$ was also observed in an antiferromagnetic XY model with frustrated boundary conditions [48]. It appears to be generic behavior for $g = g_{\mathrm{K/KI}}$ in XY models. Indeed, for this value of g, the dispersion relation, equation (19), has an expansion $\epsilon(q)^2 = a + bq^4$ for $q \to 0$ (this is equation (45) with $q = \theta_1/L$). The quartic dispersion relation implies $z = 4$.

J. Stat. Mech. (2025) 023101

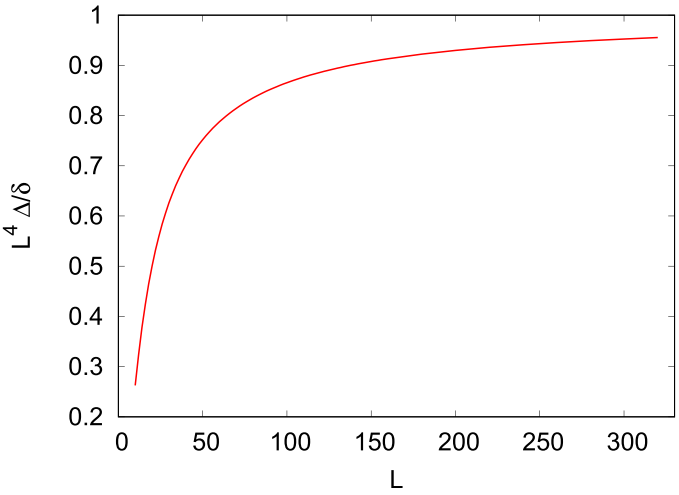

Figure 7. The ratio $\Delta(L)/\Delta_{\mathrm{K/KI}}(L)$ as a function of L for $g=0.64$, $\gamma=0.6$ and $J_0=0.8$, on the K-KI boundary. The gap $\Delta(L)$ has been obtained by a numerical diagonalization of the matrix $\hat{C}$, while $\Delta_{\mathrm{K/KI}}(L)$ is the asymptotic expression, equation (46). For these values of the parameters, $\Delta_{\mathrm{K/KI}}(L)=\delta L^{-4}$ with $\delta=1467.98$.

9.2. Crossover behavior across the K-KI boundary line

Let us now discuss the crossover behavior as the K-KI boundary is crossed by varying g at fixed γ and J_0. We parametrize the coupling g in terms of a scaling variable ϵ_{K} as

$$g=\left(1-\gamma^2\right)\left(1+\frac{\epsilon_{\mathrm{K}}}{L^{\alpha}}\right), \tag{47}$$

where α is an exponent that we determine below. We expand x_1 and x_2 as in equation (41), and substitute all expressions in the equation $\varepsilon(x_1)^2=\varepsilon(x_2)^2$. We obtain

$$-\frac{4}{L^{\alpha}}\epsilon_{\mathrm{K}}-\frac{1}{L^2}\left(\theta_1^2-x_{11}^2\right)+O\left(L^{-3}\right)=0. \tag{48}$$

Thus, nontrivial scaling behavior is obtained by taking $\alpha=2$ and requiring

$$x_{11}^2=4\epsilon_{\mathrm{K}}+\theta_1^2. \tag{49}$$

Note that, in equation (41), we are not assuming that x_{11} is real. This is correct in the K phase, but it is not valid deep in the KI phase where both x_1 and x_2 are phases.

An additional relation between x_{11} and θ_1 is obtained as before. We consider the set of equations, equation (15), set $c_2=1$ and eliminate c_1, d_1 and d_2. After a lengthy calculation, we finally obtain the equation

$$\cos\theta_1\cosh x_{11}-1=2\epsilon_{\mathrm{K}}\frac{\sin\theta_1}{\theta_1}\frac{\sinh x_{11}}{x_{11}}. \tag{50}$$

J. Stat. Mech. (2025) 023101

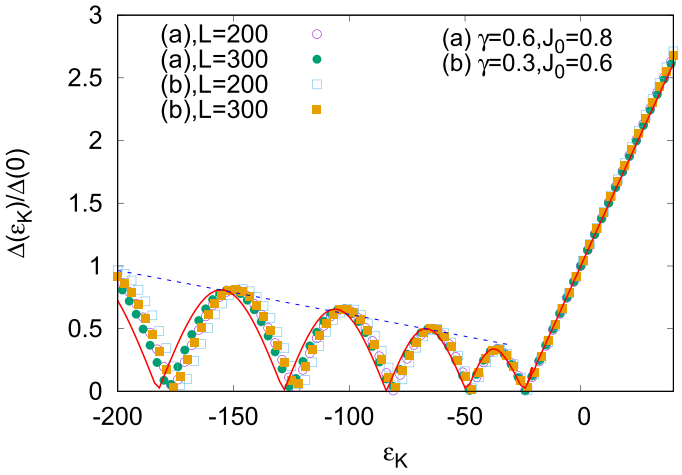

Figure 8. The crossover function across the K-KI boundary. We report the finite-size gap ratio $\Delta(\epsilon_{\rm K}, L)/\Delta(0, L)$ versus $\epsilon_{\rm K} = L^2(g/(1-\gamma^2)-1)$ for two different systems: (a) $\gamma = 0.6$, $J_0 = 0.8$; (b) $\gamma = 0.3$, $J_0 = 0.6$. The gap $\Delta(\epsilon_{\rm K}, L)$ has been obtained by a numerical diagonalization of the matrix $\hat{C}$. The solid curve is the scaling function $f_{\rm K/KI}(\epsilon_{\rm K})$. In the KI phase ($\epsilon_{\rm K} < 0$), the crossover function vanishes for $\epsilon_{\rm K} = -24.674, -49.348, -83.8916, -128.305, -182.588, \ldots$, see equation (53). The dashed line corresponds to a fit of the maxima of the scaling curve for $\epsilon_{\rm K} < -50$, see the text.

For $\epsilon_{\rm K} = 0$, we re-obtain equation (42). This equation, together with equation (49), allows one to compute x_{11} and θ_1 for each value of $\epsilon_{\rm K}$. The equations have an infinite number of solutions that are directly related to the eigenvalues of the matrix $\hat{C}$. We label the solutions as $\theta_{1,n}$ and $x_{11,n}$, $n \geqslant 1$: they are ordered so that $0 < \theta_{1,1} < \theta_{1,2} < \ldots$. The values $x_{11,n}$ and $\theta_{1,n}$ are obviously related by equation (49). As it is implicit in the notation, $\theta_{1,n}$ and $x_{11,n}$ are the values of θ_1 and x_{11} for the nth eigenvalue of the matrix $\hat{C}$. In particular, the values $x_{11,1}$ and $\theta_{1,1}$ correspond to the ground state, while $x_{11,2}$ and $\theta_{1,2}$ correspond to the first excited state.

Finally, the large-size behavior of the gap is given by

$$\Delta = \frac{\left(1-\gamma^2\right)}{2\gamma^2}\left(\theta_{1,2}^2 - \theta_{1,1}^2\right)\left(4\epsilon_{\rm K} + \theta_{1,2}^2 + \theta_{1,1}^2\right)\frac{1}{L^4}. \tag{51}$$

As it occurs for $\epsilon_{\rm K} = 0$, the gap decreases as L^{-4} for generic values of $\epsilon_{\rm K}$.

The previous results allow us to predict the scaling behavior

$$\Delta\left(\epsilon_{\rm K}, L\right) = \Delta_0\left(L\right) f_{\rm K/KI}\left(\epsilon_{\rm K}\right), \tag{52}$$

across the K-KI boundary for large values of L, where $\Delta_0(L) = \Delta_{\rm K/KI}$ is the large-size expression for the gap on the boundary line, i.e. for $\epsilon_{\rm K} = 0$, given in equation (46). In figure 8, we report the scaling curve $f_{\rm K/KI}(\epsilon_{\rm K})$ together with numerical results for two different systems. The numerical data are in good agreement with the asymptotic curve with size corrections that increase as $\epsilon_{\rm K}$ becomes more negative. The existence of a

J. Stat. Mech. (2025) 023101

universal K-KI scaling allows us to interpret the K-KI boundary as a surface of continuous transitions. Correspondingly, in the language of renormalization-group theory, g, or, more precisely, the difference $g - g_{\rm K/KI}$, plays the role of relevant perturbation of the K-KI transition, with the renormalization-group dimension $y_g = 2$.

Some general properties of the scaling curve $f_{\rm K/KI}(\epsilon_{\rm K})$ are discussed in appendix F. For positive $\epsilon_{\rm K}$ the curve is very well approximated by a straight line: $f_{\rm K/KI}(\epsilon_{\rm K}) \approx a\epsilon_{\rm K} + b$, with $a = 0.0356478$, see figure 8. For large negative values of $\epsilon_{\rm K}$, $f_{\rm K/KI}(\epsilon_{\rm K})$ behaves as $\epsilon_{\rm K}$ times an oscillating bounded function of $\epsilon_{\rm K}$. The data are consistent with this behavior: for instance, the maxima of the scaling curve for $\epsilon_{\rm K} < -50$ are well fitted by the linear function $0.264 - 0.0035\epsilon_{\rm K}$, see figure 8. Finally, the curve vanishes for

$$\epsilon_{\rm K} = -\frac{\pi^2}{2}\left(m^2 + 2m + 2\right), \tag{53}$$

where m is a positive integer.

10. Conclusions

In this work, we have considered the one-dimensional XY quantum chain in a transverse field g, see equation (1), in the presence of OBF. For $g = 1$, the model undergoes a continuous transition separating a disordered paramagnetic phase ($g > 1$) from a low-g phase, in which the bulk phase behavior depends on the boundary conditions. We determine the energy spectrum of the model. By a generalization of the approach applied to the Ising chain in [16], the problem of determining the energy spectrum for a chain of length L is reduced to the problem of solving a system of five algebraic equations in five unknowns. The analysis of the solutions of these equations gives us exact analytic results for the energy gap Δ (the energy difference between the two lowest-energy states) as a function of the model parameters for $g < 1$ and large values of L. On the basis of these results, we are able to classify the different phases occurring in the small-g regime. Four different phases emerge:

i) A magnetized (M) phase. In this case the system is ferromagnetic, with two low-lying states. The gap Δ decreases exponentially with the size, as e^{-aL}.

ii) An magnetized-incommensurate (MI) phase. Also, in this case, there are two low-lying states. The gap behaves as $\mathrm{e}^{-aL} f(L)$, where $f(L)$ is a bounded oscillating function of L. The oscillations are not commensurate with the system size.

iii) A kink (K) phase. There is a tower of low-lying delocalized states of momenta of order $1/L$, which become degenerate in the infinite-volume limit. The gap behaves as L^{-2}.

iv) A kink-incommensurate (KI) phase. Also, in this case, there is a tower of low-lying delocalized excitations that are degenerate in the infinite-volume limit. The gap behaves as $L^{-2} f(L)$, where $f(L)$ is a bounded oscillating function of L.

The M and the MI phases, with two quasidegenerate low-energy states, are the only ones present when periodic or open boundary conditions are considered, see, for

J. Stat. Mech. (2025) 023101

example [11]. The K phase was already discussed in [15] in the context of the Ising chain and it appears when the boundary fields are sufficiently strong. It can also be induced in Ising rings by sufficiently strong defects that destroy the ferromagnetic order [14]. The KI phase is a phase that is only present in the XY model for $\gamma < 1$. It has delocalized excitations as in the K phase, but it also shares, with the MI phase, the property that the gap shows incommensurate oscillations with the chain size L.

We have also discussed the behavior of the model along the boundaries that separate the different phases. References [14, 15] discussed the crossover behavior across the M-K boundary for Ising chains. Here, we perform the same calculation for the XY model, confirming the universality of the M-K crossover behavior. We have also investigated the behavior along the K-KI boundary. On the boundary, we find that the gap decreases as L^{-4}, i.e. that the dynamic critical exponent z is equal to 4. Moreover, we are able to completely characterize the crossover across the boundary, determining the relevant scaling variable and the crossover scaling function for the gap. As expected, the scaling function is universal, provided the nonuniversal normalization of the scaling variable is appropriately chosen.

In this paper we have focused on the finite-size behavior of the gap for finite chains with OBF, but results also apply to XY rings with defects with minor changes, as discussed in [14]. Moreover, it should be possible to extend these results to correlation functions, using the general techniques of [8, 9], or the perturbative approach of [15]. In particular, it would be interesting to compute the two-point correlation function and $\langle \sigma_x^{(i)} \rangle$ as a function of x. Results for the KI phase or, at least for the K-KI boundary, would provide a better understanding of the origin of the size oscillations of the gap. One could also determine the entanglement properties [49] of the phases, to understand their dependence on the boundary interactions [50], as well as the dynamic behavior under different dynamic protocols [2, 51], extending the results of [52, 53]. From a technical point of view, our method is quite general and it can also be applied to the antiferromagnetic XY model in a transverse field with different types of boundary conditions. In this case, we expect (for a discussion of these issues, see [54–56] and references therein) rich phase behavior, with different frustrated phases that can be stabilized by an appropriate choice of the boundary conditions and of the (even or odd) length of the chain. In particular, we should mention the recent results of [48] for the antiferromagnetic XY model with frustrated boundary conditions. Their model presents two phases, which we can identify with the K and KI phases discussed here and which are separated by a transition line with the dynamic exponent $z = 4$, as we observe on the K-KI boundary. It would be interesting to perform a more detailed comparison of the two models (for instance, one might compare the K-KI crossover function in the two models) to verify the expected universality.

J. Stat. Mech. (2025) 023101

Acknowledgment

A P acknowledges support from Project PRIN 2022 'Emerging gauge theories: critical properties and quantum dynamics' (20227JZKWP).

Appendix A. Jordan–Wigner representation and Hamiltonian diagonalization

To compute the spectrum of Hamiltonian (5), we follow [3]. We first perform a Jordan–Wigner transformation, defining the fermionic operators c_i and $c_i^\dagger$,

$$c_i^\dagger = R_i\,\sigma_i^+, \qquad c_i = R_i\,\sigma_i^-, \qquad R_i = (-1)^{i-1}\prod_{j=0}^{i-1}\sigma_j^{(3)}, \tag{A.1}$$

where $\sigma^\pm = (\sigma^{(1)} \pm i\sigma^{(2)})/2$. These relations can be inverted, obtaining

$$\sigma_i^{(1)} = R_i\left(c_i^\dagger + c_i\right), \qquad \sigma_i^{(2)} = -i\,R_i\left(c_i^\dagger - c_i\right), \qquad \sigma_i^{(3)} = 2c_i^\dagger c_i - 1. \tag{A.2}$$

In terms of the fermionic operators, Hamiltonian (5) becomes

$$\begin{aligned} H_e = &-\sum_{i=1}^{L-1}\left[c_{i+1}^\dagger c_i + c_i^\dagger c_{i+1} + \gamma\left(c_i^\dagger c_{i+1}^\dagger - c_i^\dagger c_{i+1}\right)\right] - g\sum_{i=1}^{L}\left(2c_i^\dagger c_i - 1\right) \\ &- \sum_{i=0,L} J_i\left(c_{i+1}^\dagger c_i + c_i^\dagger c_{i+1} + c_i^\dagger c_{i+1}^\dagger + c_{i+1}c_i\right) \end{aligned} \tag{A.3}$$

where the last term is the boundary contribution (i takes the values 0 and L only). The previous expression can be rewritten in the more compact form

$$H_e = Lg - \sum_{i,j=0}^{L+1}\left[c_i^\dagger A_{ij} c_j + \frac{1}{2}c_i^\dagger B_{ij} c_j^\dagger + \frac{1}{2}c_i B_{ij} c_j\right], \tag{A.4}$$

where the matrices A and B are symmetric and antisymmetric, respectively. Finally, we perform a Bogoliubov transformation, introducing new canonical fermionic variables

$$\eta_k = \sum_{i=0}^{L+1}\left(g_{ki}c_i^\dagger + h_{ki}c_i\right), \tag{A.5}$$

where g_{ki} and h_{ki} are fixed by the requirement that H_e takes the form

$$H_e = E_{gs} + \sum_{k=0}^{L+1}\mathcal{E}_k\eta_k^\dagger\eta_k, \tag{A.6}$$

with $0 \leqslant \mathcal{E}_0 \leqslant \mathcal{E}_1 \leqslant \ldots$. Following [3], we define the vectors

$$U_k = (g_{k0} + h_{k0}, g_{k1} + h_{k1}, \ldots), \qquad V_k = (g_{k0} - h_{k0}, g_{k1} - h_{k1}, \ldots). \tag{A.7}$$

J. Stat. Mech. (2025) 023101

The variables η_k satisfy canonical anticommutation relations if the vectors U_k form an orthonormal basis, and so does the set V_k. The vectors V_k satisfy

$$(A+B)(A-B)V_k = \mathcal{E}_k^2 V_k. \tag{A.8}$$

Thus, if we define $C=(A+B)(A-B)$, the determination of the energies $\mathcal{E}_k$ is equivalent to the determination of the eigenvalues of the matrix C. Note that the Hamiltonian H_e is invariant under a parity transformation generated by $P_z = \prod_{i=0}^{L+1} \sigma_i^{(3)}$). Note also that the spectrum is doubly degenerate. This implies that C has, necessarily, a zero eigenvalue. The matrix C is given in equation (8) in the text.

The previous calculations allow us to obtain the spectrum of H_e. We should now discuss how to use these results to obtain the spectrum of H in the presence of OBF. Let us first note that the Hamiltonian H_e commutes with both $\sigma_0^{(1)}$ and $\sigma_{L+1}^{(1)}$, which can therefore be simultaneously diagonalized. The Hilbert space can be divided into four sectors, which we label as $(1,1)$, $(-1,1)$, $(1,-1)$ and $(-1,-1)$, where (s_0, s_{L+1}) are the eigenvalues of $\sigma_0^{(1)}$ and $\sigma_{L+1}^{(1)}$. The restriction of H_e to each sector gives rise to the Hamiltonian H, defined in equation (1), with a boundary term of the form in equation (2). In particular, the restriction to the sector $(1,-1)$ gives the spectrum in the presence of OBF, while the restriction to the sector (1,1) gives the spectrum with parallel boundary fields. To conclude the calculation we should determine the states that belong to the sector $(1,-1)$. The analysis is reported in [15]. In the sector $s_0=1$, $s_{L+1}=-1$, the lowest-energy state is the first excited state $\eta_1^\dagger|0\rangle$ of the Hamiltonian H_e and all states are obtained as $\eta_{k_1}^\dagger \ldots \eta_{k_m}^\dagger |0\rangle$ with $k_i \geqslant 1$ and m odd. In particular, the first excited state in the sector is $\eta_2^\dagger|0\rangle$, so that the energy gap is $\Delta = \mathcal{E}_2 - \mathcal{E}_1$.

Appendix B. Consistency of the parametrization of the eigenvectors

In section 4, we proved that a vector of the form in equation (14) is an eigenvector of $\hat{C}$ if the coefficients c_1, c_2, d_1 and d_2 satisfy equation (15) and $\varepsilon(x_1)^2 = \varepsilon(x_2)^2$. In this appendix, we wish to prove the opposite result: any eigenvector of $\hat{C}$ can be written as in equation (14) with appropriate coefficients c_1, c_2, d_1, d_2, x_1 and x_2.

Let us consider an eigenvector ϕ_L of $\hat{C}$ with eigenvalue $\mathcal{E}^2$. We wish to show that we can determine c_1, c_2, d_1, d_2, x_1 and x_2, so that $\psi_L = \phi_L$. We first determine x_1 and x_2 so that $\varepsilon(x_1)^2 = \varepsilon(x_2)^2 = \mathcal{E}^2$ (this is discussed in detail in section 5). Then, we determine c_1, c_2, d_1 and d_2 by solving the linear system of equations $\psi_{L,i} = \phi_{L,i}$ for $i = 1,2,3,4$.

We now wish to prove that the resulting vector ψ_L is equal to ϕ_L, i.e. that $\psi_{L,i} = \phi_{L,i}$ for $i \geqslant 5$. Let us notice that equation (15) can be reinterpreted as a recursion relation for the vector components. For $k \geqslant 5$, taking into account the particular structure of $\hat{C}$, we can write

$$\mathrm{Eq}_{k-2} = \sum_{i=k-4}^{k} \hat{C}_{k-2,i}\psi_{L,i} - \mathcal{E}^2 \psi_{L,k-2} = 0, \tag{B.1}$$

J. Stat. Mech. (2025) 023101

which gives

$$\psi_{L,k} = \frac{1}{\hat{C}_{k-2,k}} \left[\mathcal{E}^2 \psi_{L,k-2} - \sum_{i=k-4}^{k-1} \hat{C}_{k-2,i} \psi_{L,i} \right]. \tag{B.2}$$

Since the parametrization, equation (14), satisfies $\mathrm{Eq}_k = 0$ for $3 \leqslant k \leqslant L-1$ (therefore, $\mathrm{Eq}_{k-2} = 0$ holds for $5 \leqslant k \leqslant L+1$), we can use equation (B.2) to determine all components $\psi_{L,k}$, $k \geqslant 5$, in terms of $\psi_{L,i}$ with $i = 1,2,3,4$. Recursion (B.2) (with ϕ replacing ψ) also holds for ϕ_L (it satisfies $\mathrm{Eq}_k = 0$ for any k) and thus the same recursion gives $\phi_{L,k}$ in terms of $\phi_{L,i}$ with $i = 1,2,3,4$. It is then enough to note that the starting values of the recursion are the same ($\psi_{L,i} = \phi_{L,i}$ for $i = 1,...,4$) to conclude that $\phi_{L,k} = \psi_{L,k}$ for any k.

Appendix C. Magnetized phases: determination of the parameters x_i

In this appendix we wish to determine the values that x_1 and x_2 take for $L \to \infty$, when the system is in a magnetized phase. Here, x_1 and x_2 always refer to the (degenerate) ground state.

As discussed in section 5, in the magnetized phases, $|x_1|$ and $|x_2|$ are both larger than 1. Therefore, for large system sizes, the quantities x_1^{-L} and x_2^{-L} are exponentially small and thus the leading behavior is obtained by neglecting these terms[6]. Equations (15) decouple: Eq_1 and Eq_2 depend only on c_1 and c_2, while Eq_L and Eq_{L+1} depend only d_1 and d_2.

There are two classes of solutions of $\mathrm{Eq}_L = 0$ and $\mathrm{Eq}_{L+1} = 0$. First, there is the trivial solution $d_1 = d_2 = 0$. If this is not the case, we obtain

$$d_2 = -\left(\frac{x_1}{x_2}\right)^3 d_1 \tag{C.1}$$

and the relation

$$x_1 x_2 = \frac{(1+\gamma)^2 - 4J_0^2}{1-\gamma^2}. \tag{C.2}$$

Equations $\mathrm{Eq}_1 = 0$ and $\mathrm{Eq}_2 = 0$ have a larger set of solutions. Beside the trivial solution $c_1 = c_2 = 0$, we have four different possibilities:

- $c_1 = 0$ and $f_1(x_2) = 0$, with $f_1(x_1) \neq 0$;
- $c_2 = 0$ and $f_1(x_1) = 0$, with $f_1(x_2) \neq 0$;
- $f_1(x_1) = 0$ and $f_1(x_2) = 0$;

[6] More precisely, these terms can be neglected provided that the coefficients c_i and d_i do not increase exponentially with the system size. We have verified this assumption numerically: we compute the eigenvectors by diagonalizing the matrix $\hat{C}$ and then determine the coefficients c_1, c_2, d_1 and d_2 as explained in appendix B. The analytic results presented in this appendix are consistent with this assumption.

J. Stat. Mech. (2025) 023101

- x_1 and x_2 satisfy equation (C.2) and

$$c_2 = -c_1 \frac{x_1\left[1-\gamma-2gx_1+(1+\gamma)x_1^2\right]}{x_2\left[1-\gamma-2gx_2+(1+\gamma)x_2^2\right]}. \tag{C.3}$$

Here, the function $f_1(x)$ is defined as

$$f_1(x) = (1+\gamma)x^2 - 2gx + (1-\gamma) = 0. \tag{C.4}$$

Finally, we should determine the additional constraints due to the fact that x_1 and x_2 should satisfy the equation $\varepsilon(x_1)^2 = \varepsilon(x_2)^2$, which we rewrite in the more convenient form

$$x_1^2 x_2^2\left[\varepsilon(x_1)^2 - \varepsilon(x_2)^2\right] = 0. \tag{C.5}$$

Let us first assume that x_1 and x_2 satisfy equation (C.2). We rewrite each term $x_1^a x_2^b$ as $(x_1x_2)^K x_1^{a-K} x_2^{b-K}$, with $K = \min(a,b)$ and then we use equation (C.2) for x_1x_2. Equation (C.5) drastically simplifies, allowing us to obtain

$$x_1 + x_2 = \frac{2g\left[(1+\gamma)^2 - 4J_0^2\right]}{(1-\gamma^2)(1+\gamma-2J_0^2)}. \tag{C.6}$$

A second possibility is that x_1 satisfies $f_1(x_1) = 0$. If this is the case, we obtain that x_2 satisfies either $f_1(x_2) = 0$ or $f_1(1/x_2) = 0$. Analogously, if $f_1(x_2) = 0$, x_1 satisfies either $f_1(x_1) = 0$ or $f_1(1/x_1) = 0$. Combining all the results, we conclude that there are two possibilities for x_1 and x_2 in the magnetized phase. They should satisfy one of these two conditions:

- equations (C.2) and (C.6);
- $f_1(x_i)f_1(1/x_i) = 0$ for both x_1 and x_2.

We have not been able to understand analytically which of the two conditions is the relevant one for each value of the parameters g, γ and J_0, and we have thus performed a numerical analysis, as discussed in section 5. We numerically determine the eigenvalues of the matrix $\hat{C}$, and then obtain the values x_1 and x_2 for the ground state by solving $\varepsilon(x)^2 = \mathcal{E}_1^2$. Finally, we check which of the two conditions is satisfied. The result is particularly simple. For $\gamma > 0$, x_1 and x_2 satisfy equations (C.2) and (C.6). On the other hand, for $\gamma < 0$, x_1 and x_2 both satisfy $f_1(x_i)f_1(1/x_i) = 0$.

The previous equations allow us to determine x_1 and x_2, as long as they both satisfy $|x_i| > 1$. If the solutions are both real and larger than 1 in absolute value, the system is in the M phase for the given set of parameters. If they are complex conjugate with $|x_1| = |x_2| > 1$, the system is in the MI phase.

It is important to note that we obtain a two-dimensional space of solutions. Indeed, if x_1 and x_2 are computed by using equations (C.2) and (C.6), we can arbitrarily fix c_1 and d_1 and compute c_2 and d_2 using equations (C.1) and (C.3). On the other hand, if $f_1(x_i)f_1(1/x_i) = 0$, we should set $d_1 = d_2 = 0$ and arbitrarily choose c_1 and c_2, or,

J. Stat. Mech. (2025) 023101

viceversa, set $c_1 = c_2 = 0$ and choose d_1 and d_2. Therefore, if we neglect exponentially small terms, the solutions form a degenerate two-dimensional space. This is exactly the expected behavior for the two lowest-energy states in a magnetized phase. The degeneracy is lifted for finite values of L. To compute the splitting, one should consider the terms of order x_1^{-L} and x_2^{-L}. Since $|x_2| < |x_1|$, the dominant contribution is due to x_2. We thus predict the gap to scale as $|x_2|^{-L}$, with incommensurate oscillations if x_2 is complex.

Appendix D. The kink phase

To determine the behavior of the gap in the kink phase in which x_1 is real and larger than 1 in absolute value, and $x_2 = \mathrm{e}^{\mathrm{i}\phi}$, we have first performed a numerical study of the size behavior of the phase ϕ. We diagonalize $\hat{C}$ and then compute $x_{1,n}(L)$ and $x_{2,n}(L)$ for the low-lying energy states (the 'kink' states) by solving the equation $\varepsilon(x)^2 = \mathcal{E}_n$. We find that for all these states ϕ vanishes in the infinite-size limit as $1/L$, i.e. $\phi_n \approx \theta_{1.n}/L$ for large sizes (as usual, the suffix n indicates that ϕ_n is the values of ϕ for the nth eigenvalue of the matrix $\hat{C}$). Moreover, inside the kink phase, $\theta_{1,n}$ never vanishes.

On the basis of these numerical results, we parametrize ϕ for the lowest-lying states as

$$\phi = \frac{\theta_1}{L} + \frac{\theta_2}{L^2} + O\left(L^{-3}\right). \tag{D.1}$$

This specific behavior of x_2 allows us to determine x_1 in the infinite-size limit from the equation $\varepsilon(x_1)^2 = \varepsilon(x_2)^2$. Setting $x_2 = 1$, we obtain

$$x_1 = x_{10} \equiv \frac{1}{1-\gamma^2}\left[2\sqrt{g(\gamma^2+g-1)} + \gamma^2 + 2g - 1\right], \tag{D.2}$$

a result that is fully supported by the numerical results obtained by the direct diagonalization of $\hat{C}$. Corrections decay as $1/L^2$, as described below.

To determine the correction term θ_1, we expand x_1 as

$$x_1 \approx x_{10} + \frac{x_{11}}{L} + \frac{x_{12}}{L^2}. \tag{D.3}$$

Substituting this expansion and equation (D.1) in the equation $\varepsilon(x_1)^2 = \varepsilon(x_2)^2$, we obtain $x_{11} = 0$ at the order $1/L$, and $x_{12} = A\theta_1^2$ (A is a function of g and γ) at the order $1/L^2$. Thus, at the order $1/L$ we can approximate x_1 with the leading term x_{10}. Then, we consider the four equations $\mathrm{Eq}_k = 0$ reported in equation (15). We drop the terms that are proportional to x_1^{-L}, which are exponentially small (in the kink phase $|x_1| > 1$) and replace x_1 with x_{10}. The coefficients c_1, c_2, d_1 and d_2 can be determined up to a multiplicative constant (the normalization of ψ). We have numerically verified that c_2 never vanishes for generic values of the parameters in the kink phase, and therefore we can use the above freedom to set $c_2 = 1$. Then, we solve the linear equations $\mathrm{Eq}_2 = 0$, $\mathrm{Eq}_L = 0$ and $\mathrm{Eq}_{L+1} = 0$ in terms of c_1, d_1 and d_2 and substitute the results in $\mathrm{Eq}_1 = 0$. The equation depends on x_2 and x_2^{-L}. If we now take the limit $L \to \infty$ and use

J. Stat. Mech. (2025) 023101

the expansion of x_2, we obtain the condition

$$A\left(g,\gamma,J_0\right)\sin\theta_1=0, \tag{D.4}$$

where $A(g,\gamma,J_0)$ is a nontrivial function of the parameters. It implies

$$\theta_1=k\pi \qquad \phi=\frac{k\pi}{L}+O\left(L^{-2}\right). \tag{D.5}$$

It is not restrictive to assume that $\phi\geqslant 0$, so that k is a nonnegative integer. We will now argue that, for generic points in the kink phase, k should be strictly positive. More precisely, for the nth eigenvalue we have $\theta_{1,n}=n\pi$. This result is the same as that obtained in the kink phase of the Ising chain with $\gamma=1$ [15].

To show that θ_1 cannot be zero, we combine numerical and analytic results. Let us suppose the opposite, assuming that $\phi\approx\theta_k/L^k$ for large L, with $k\geqslant 2$. Equation $\mathrm{Eq}_1=0$ gives

$$B\left(g,\gamma,J_0\right)\theta_n L^{1-n}+O\left(L^{-n}\right)=0, \tag{D.6}$$

implying $\theta_k=0$. Thus, if $\theta_1=0$, ϕ should decrease faster than any power of L (most probably exponentially) which, in turn, would imply $x_1=x_{10}$, $x_2=1$ with corrections that decrease faster than any power of L. As already mentioned, the numerical analysis reported at the beginning of this appendix allows us to exclude this type of behavior inside the kink phase. Thus, in the kink phase, we should only consider positive integer values of k, as was proved rigorously for the Ising chain [15]. We have thus fully characterized the values of x_1 and x_2 that correspond to the eigenvectors of $\hat{C}$.

Relations (D.2) and (D.5) also hold on the boundary between the M phase and the K phase, see equation (28). However, numerically we find that $x_2=1$ with essentially no corrections for the lowest-energy state (eigenvalue $\mathcal{E}_1^2$), implying $\theta_{1,1}=0$. Higher-energy eigenstates correspond to $\theta_{1,n}=(n-1)\pi$ with $n>1$. This different behavior for points inside the K phase and on the boundary K-M is not surprising, as the same occurs in the Ising chain (for this model, analytic proof is given in [15]).

Appendix E. The magnetized-kink boundary

In this appendix we wish to show the validity of equation (39) along the whole M-K boundary and, in particular, we wish to compute the constant R so that the scaling curve $f_\Delta(\zeta_s)$ is the same as that computed in [15]. This result proves the universality of the M-K crossover.

To determine the gap scaling function we should determine the relation between x_1,x_2 and the scaling variable ζ_s. For this purpose we proceed as in appendix D. We expand x_1 and x_2 as

$$x_1=x_{1,\mathrm{K/M}}+\frac{x_{11}}{L}+O\left(L^{-2}\right), \qquad x_2=1+\frac{i\theta_1}{L}+O\left(L^{-2}\right) \tag{E.1}$$

J. Stat. Mech. (2025) 023101

and set $J_0 = J_{0c} + \epsilon/L$. Note that we have included a factor i in the expansion of x_2, to make the expansion look similar to that performed in [15] (θ_1 corresponds to k in [15]). However, we are not assuming θ_1 to be real: θ_1 will be purely imaginary in the magnetized phase.

As in appendix D, we first verify that $x_{11} = 0$, so that, at the order $1/L$, we can replace x_1 with $x_{1,\mathrm{K/M}}$ in all the equations in equation (15). Then, we set $c_2 = 1$, determine c_1, d_1 and d_2 using three of the four equations in equation (15), and substitute the result in the equation $\mathrm{Eq}_1 = 0$. The calculation is quite involved. At the end, we obtain an equation of the form

$$A\epsilon\theta_1 \cos\theta_1 + B\theta_1^2 \sin\theta_1 + C\epsilon^2 \sin\theta_1 = 0, \tag{E.2}$$

where A, B, C are complicated functions of the model parameters. This equation relates θ_1 with the parameter ϵ.

We would now like to show that, by an appropriate choice of the constant R defined in equation (38), we can re-express this relation as in [15]:

$$4\zeta_s\theta_1 + \left(4\zeta_s^2 - \theta_1^2\right)\tan\theta_1 = 0. \tag{E.3}$$

This would prove that the scaling functions for the XY model are the same as those computed for the Ising chain.

Equations (E.2) and (E.3) look similar. By comparing the two expressions, we find that it is possible to rewrite equation (E.2) as equation (E.3) via an appropriate choice of R, only if A, B and C satisfy the relation

$$A = -2\sqrt{-BC}. \tag{E.4}$$

We have not been able to verify relation (E.4) analytically. We have therefore performed a numerical check. We have considered 100 different boundary points, finding that equation (E.4) is verified to machine precision in all cases. If relation (E.4) holds, the crossover function is universal, provided the constant R is

$$R = \frac{1}{2}\sqrt{-\frac{C}{B}}. \tag{E.5}$$

We have not been able to analytically simplify the expression (E.5). We will now derive R differently, assuming that universality holds and using the results of [15]. This quick and simple method provides a significantly simpler expression for the constant. For $\zeta_s \to -\infty$, i.e. deep in the magnetized phase, the scaling function can be expanded as (see [15])

$$f_\Delta(\zeta_s) = \frac{32}{\pi^2}\zeta_s^2 \mathrm{e}^{2\zeta_s} = \frac{32}{\pi^2}R^2L^2\left(J_0 - J_{0c}\right)^2 \mathrm{e}^{2RL(J_0 - J_{0c})}. \tag{E.6}$$

J. Stat. Mech. (2025) 023101

In the M phase, we expect $\Delta(J) = a x_2^{-L}$ (a depends on all model parameters), while $\Delta(J_{0c}) = b/L^2$, so that

$$f_\Delta(\zeta_s) = \frac{a}{b} L^2 \mathrm{e}^{-L \ln x_2}. \tag{E.7}$$

Comparing the two expressions, we obtain

$$\ln x_2 = -2R(J_0 - J_{0c}) \tag{E.8}$$

in the limit $J_0 \to J_{0c}$. Expanding x_2 (obtained by solving equations (20) and (21)) close to the point $J_0 = J_{0c}$, this relation gives equation (40).

Appendix F. Properties of the K-KI crossover function

The scaling curve $f_{\mathrm{K/KI}}(\epsilon_{\mathrm{K}})$ defined in equation (52) shows two different types of behavior. For positive ϵ_{K} the curve is essentially a straight line. This linear behavior can be predicted by noting that $\Delta(\epsilon_{\mathrm{K}})$, computed for $\epsilon_{\mathrm{K}} \to \infty$ (deep in the K phase), should reproduce equation (34) computed in the limit $g \to 1 - \gamma^2$ (close to the boundary). This implies $f_{\mathrm{K/KI}}(\epsilon_{\mathrm{K}}) \approx a\epsilon_{\mathrm{K}}$ for $\epsilon_{\mathrm{K}} \to \infty$, with

$$a = \frac{12\pi^2}{\theta_{1,2}^4 - \theta_{1,1}^4} \approx 0.0356478. \tag{F.1}$$

where $\theta_{1,2}$ and $\theta_{1,1}$ are the phases on the K-KI boundary, i.e. for $\epsilon_{\mathrm{K}} = 0$, see equations (43) and (44).[7]

The approximately linear behavior is observed as long as $x_{11,1}$ and $x_{11,2}$ are both real and positive. When one or both become complex, the behavior changes. To determine the values $\epsilon_{\mathrm{K},n}$ of ϵ_{K} where $x_{11,n} = 0$, we first note that the values $x_{11,n}$ are all positive for $\epsilon_{\mathrm{K}} > 0$. If we decrease ϵ_{K}, the parameters $x_{11,n}$ decrease, as expected on the basis of equation (49). Therefore, there is a value ϵ_{K} (a different one for each n, that we indicate with $\epsilon_{\mathrm{K},n}$), for which $x_{11,n} = 0$. If ϵ_{K} is further decreased, $x_{11,n}$ becomes complex. To determine the values of ϵ_{K} for which there is a solution with $x_{11} = 0$, we set $x_{11} = 0$ in equation (49), which gives $\epsilon_{\mathrm{K}} = -\theta_1^2/4$. Then equation (50) becomes

$$1 - \cos\theta_1 = \frac{\theta_1}{2} \sin\theta_1. \tag{F.2}$$

There are two classes of solutions of this equation: (i) $\theta_1 = 2k\pi$; and (ii) the solutions of $\tan\theta_1/2 = \theta_1/2$. To understand the relation between these solutions and the values $\theta_{1,n}$, we have performed a numerical analysis, finding that each solution of equation (F.2) corresponds to a different eigenvalue of the matrix $\hat{C}$. For $\theta_1 = 2\pi$, we find that the lowest-energy $x_{11,1}$ vanishes. Thus, $\theta_{1,1} = 2\pi$ and $\epsilon_{K,1} = -\pi^2 = -9.8696$. The second smallest θ_1 that is a solution of equation (F.2) is $\theta_1 = 8.98682$ (the smallest θ_1 that is a solution of type (ii)). It corresponds to $x_{11,2} = 0$, so that $\epsilon_{K,2} = -20.1907$. We thus conclude that all

[7] As before, $x_{11,n}$ and $\theta_{1,n}$ indicate the values of x_{11} and of θ_1 for the nth eigenstate of the matrix $\hat{C}$.

J. Stat. Mech. (2025) 023101

$x_{11,n}$ are positive and real for $\epsilon_{\rm K} > \epsilon_{K,1} = -9.8696$, while, for $-20.1907 < \epsilon_{\rm K} < -9.8696$, $x_{11,1}$ is complex and $x_{11,2}$ (and also $x_{11,n}$, $n > 2$) is real. For $\epsilon_{\rm K} < -20.1907$, x_{11} is purely imaginary both for the ground state and for the first excited state. In this regime, the scaling function shows expected oscillatory behavior.

A second interesting property of the scaling function is that it vanishes on a sequence of values of $\epsilon_{\rm K}$, where $\theta_{1,1} = \theta_{1,2}$, i.e. the correction term is the same for the ground state and the first excited state. To determine these points, let us rewrite equation (50) as $f(\theta_1) = 0$, replacing x_{11} with the expression obtained using equation (49). The solutions, such that $\theta_{1,1} = \theta_{1,2}$, should also satisfy $f'(\theta_1) = 0$, a condition that can be written as

$$\begin{aligned}&\left(\theta_1^2 + x_{11}^2\right)\left(\cos\theta_1 \cosh x_{11} - 1\right) \\ &\quad + x_{11}\left(\theta_1^2 - 2\epsilon_{\rm K}\right)\cos\theta_1 \sinh x_{11} - \theta_1\left(x_{11}^2 + 2\epsilon_{\rm K}\right)\sin\theta_1 \cosh x_{11} = 0.\end{aligned} \tag{F.3}$$

Thus, the values of $\epsilon_{\rm K}$ where the phases of two different eigenstates coincide, i.e. $\theta_{1,n} = \theta_{1,n+1}$ for some n, can be determined by solving equations (49), (50) and (F.3) in terms of θ_1, x_{11} and $\epsilon_{\rm K}$. By inspection, it is immediate to verify that $\theta_1 = 2\pi m_1$, $x_{11} = 2\pi m_2 i$, $\epsilon_{\rm K} = -\pi^2(m_1^2 + m_2^2)$ is a solution for any integer m_1 and m_2. Numerically, we have verified that all solutions that correspond to $\theta_{1,1} = \theta_{1,2}$ belong to this class. More precisely, they are a subset with $m_1 = m_2 + 2$. Therefore, the points with vanishing L^{-4} correction correspond to

$$\epsilon_{\rm K} = -\frac{\pi^2}{2}\left(m^2 + 2m + 2\right), \tag{F.4}$$

where m is a positive integer. For these values of $\epsilon_{\rm K}$, $\theta_{1,1} = \theta_{1,2} = 2\pi(m+2)$ and $x_{1,1} = x_{1,2} = 2\pi m i$.

Finally, let us discuss the behavior of the scaling function in the limit $\epsilon_{\rm K} \to -\infty$, i.e. deep in the KI phase. To obtain analytic results, we should use exact results for the gap in the KI phase. Unfortunately, we have not been able to determine the exact asymptotic behavior of the gap in this limit. Numerically, we find that the gap decreases as $L^{-2} f(L)$, where $f(L)$ is an oscillatory function, see, for example, the upper left panel in figure 5. If this is correct, we conclude that $f_{\rm K/KI}(\epsilon_{\rm K})$ behaves as $\epsilon_{\rm K}$ times an oscillating bounded function of $\epsilon_{\rm K}$ for $\epsilon_{\rm K} \to -\infty$. The data are consistent with this behavior: for instance, the maxima of the scaling curve for $\epsilon_{\rm K} < -50$ are well fitted by the linear function $0.264 - 0.0035\epsilon_{\rm K}$: see figure 8 in the text.

References

[1] Campostrini M, Pelissetto A and Vicari E 2014 Finite-size scaling at quantum transitions *Phys. Rev.* B **89** 094516

[2] Pelissetto A and Vicari E 2024 Scaling behaviors at quantum and classical first-order transitions in fifty years of the renormalization group *Fifty Years of the Renormalization Group. Dedicated to the Memory of Michael E. Fisher* ed Aharony, A O Entin-Wohlman, D Huse and L Radzihovsky (World Scientific)

[3] Lieb E, Schultz T and Mattis D 1961 Two soluble models of an antiferromagnetic chain *Ann. Phys. (NY)* **16** 407

[4] Katsura S 1962 Statistical mechanics of the anisotropic linear Heisenberg model *Phys. Rev.* **127** 1508

J. Stat. Mech. (2025) 023101

[5] Niemeijer T 1967 Some exact calculations on a chain of spins 1/2 *Physica* **36** 377
[6] Niemeijer T 1968 Some exact calculations on a chain of spins 1/2, II *Physica* **39** 313
[7] Pfeuty P 1970 The one-dimensional Ising model with a transverse field *Ann. Phys. (NY)* **57** 79
[8] Barouch E, Mc Coy B M and Dresden M 1970 Statistical mechanics of the XY Model. I *Phys. Rev.* A **2** 1075
[9] Barouch E and Mc Coy B M 1971 Statistical mechanics of the XY model II spin-correlation functions *Phys. Rev.* A **3** 786
[10] Suzuki M 1971 Equivalence of the two-dimensional Ising model to the ground state of the linear XY-model *Phys. Lett.* A **34** 94
[11] Franchini F 2017 *An introduction to integrable techniques for one-dimensional quantum systems Lecture Notes in Physics* vol 940 (Springer)
[12] Kurmann J, Thomas H and Müller G 1982 Antiferromagnetic long-range order in the anisotropic quantum spin chain *Physica* A **112** 235
[13] Müller G and Shrock R E 1985 Implications of direct-product ground states in the one-dimensional quantum XYZ and XY spin chains *Phys. Rev.* B **32** 5845
[14] Campostrini M, Pelissetto A and Vicari E 2015 Quantum transitions driven by one-bond defects in quantum Ising rings *Phys. Rev.* E **91** 042123
[15] Campostrini M, Pelissetto A and Vicari E E 2015 Quantum Ising chains with boundary fields *J. Stat. Mech.: Theory Expt.* 11015
[16] Hu K and Wu X 2021 First- and second-order quantum phase transitions in the one-dimensional transverse-field Ising model with boundary fields *Phys. Rev.* B **103** 024409
[17] Sachdev S 1999 *Quantum Phase Transitions* (Cambridge University Press)
[18] Dietrich S 1988 *Wetting Phenomena in Phase Transitions and Critical Phenomena* vol 12, ed C Domb and J L Lebowitz (Academic)
[19] Indekeu J O 1994 Line tension at wetting *Int. J. Mod. Phys.* B **8** 309
[20] Bonn D and Ross D 2001 Wetting transitions *Rep. Prog. Phys.* **64** 1085
[21] Binder K, Landau D P and Müller M 2003 Monte Carlo studies of wetting, interface localization and capillary condensation *J. Stat. Phys.* **110** 1411
[22] Abraham D B 1980 Solvable model with a roughening transition for a planar Ising ferromagnet *Phys. Rev. Lett.* **44** 1165
[23] Nakanishi H and Fisher M E 1982 Multicriticality of wetting, prewetting and surface transitions *Phys. Rev. Lett.* **49** 1565
[24] Ciach A 1986 Correlation functions in the solid-on-solid model of the fluctuating interface *Phys. Rev.* B **34** 1932
[25] Ciach A and Stecki J 1987 Scaling in the solid-on-solid interface *J. Phys. A: Math. Gen.* **20** 5619
[26] Privman V and Švrakić N M 1988 Finite-size scaling for the restricted solid-on-solid model of the two-dimensional wetting transition *Phys. Rev.* B **37** 3713
[27] Parry A O and Evans R 1990 Influence of wetting on phase equilibria: a novel mechanism for critical-point shifts in films *Phys. Rev. Lett.* **64** 439
[28] Parry A O, Evans R and Nicolaides D B 1991 Long-ranged surface perturbations for confined fluids *Phys. Rev. Lett.* **67** 2978
[29] Stecki J, Maciołek A and Olaussen K 1994 Magnetization profiles of the planar fluctuating interface in a $d=2$ Ising strip *Phys. Rev.* B **49** 1092
[30] Maciołek A and Stecki J 1996 $d=2$ Ising strip with two surface fields solved using the transfer-matrix method *Phys. Rev.* B **54** 1128
[31] Maciołek A 1996 Magnetization profiles for a $d=2$ Ising strip with opposite surface fields *J. Phys. A: Math. Gen.* **29** 3837
[32] Abraham D B and Maciołek A 2010 Casimir interactions in Ising strips with boundary fields: exact results *Phys. Rev. Lett.* **105** 055701
[33] Boccara N and Sarma G 1974 Does magnetic surface order exist? *J. Phys Lett.* **35** 95
[34] Cabrera G G and Jullien R 1986 Universality of finite-size scaling: the role of the boundary conditions *Phys. Rev. Lett.* **57** 393
Cabrera G G and Jullien R 1987 Role of boundary conditions in the finite-size Ising model *Phys. Rev.* B **35** 7062
[35] Barber M N and Cates M E 1987 Effect of boundary conditions on the finite-size transverse Ising model *Phys. Rev.* B **36** 2024
[36] Henkel M 1987 Finite-size scaling and universality in the spectrum of the quantum Ising chain. 1 Periodic and antiperiodic boundary conditions *J. Phys. A: Math. Gen.* **20** 995
[37] Burkhardt T W and Guim I 1987 Universal scaling form of the correlation length in Ising strips with periodic, free, fixed and mixed boundary conditions *Phys. Rev.* B **35** 1799

J. Stat. Mech. (2025) 023101

[38] Berche B and Turban L 1990 Inhomogeneous Ising chain in a transverse field. Finite-size scaling and asymptotic conformal spectrum *J. Phys. A: Math. Gen.* **23** 3029
[39] Turban L and Berche B 1993 Surface magnetization of aperiodic Ising quantum chains *Z. Phys.* B **92** 307
[40] Igloi F, Peschel I and Turban L 1993 Inhomogeneous systems with unusual critical behaviour *Adv. Phys.* **42** 683
[41] Karevski D 2000 Surface and bulk critical behaviour of the XY chain in a transverse field *J. Phys. A: Math. Gen.* **33** L313
[42] Izmailian N S and Hu C K 2001 Exact universal amplitude ratios for two-dimensional Ising models and a quantum spin chain *Phys Rev. Lett.* **86** 5160
[43] Dutta A, Divakaran U, Sen D, Chakrabarti B K, Rosenbaum T F and Aeppli G 2010 Quantum phase transitions in transverse field spin models: from statistical physics to quantum information (arXiv:0801.4134)
Dutta A, Aeppli G, Chakrabarti B K, Divakaran U, Rosenbaum T F and Sen D 2015 *Quantum Phase Transitions in Transverse Field Spin Models: From Statistical Physics to Quantum Information* (Cambridge University Press)
[44] Peschel I 2004 On the entanglement entropy for an XY spin chain *J. Stat. Mech.: Theory Exp.* **2004** 12005
[45] Izmailian N S and Hu C-K 2009 Boundary conditions and amplitude ratios for finite-size corrections of a one-dimensional quantum spin model *Nucl. Phys.* B **808** 613
[46] Hu K and Wu X 2023 Wetting transition in the transverse field spin-$\frac{1}{2}$ XY model with boundary fields *Phys. Rev.* B **107** 134433
[47] Catalano A G, Brtan D, Franchini F and Giampaolo S M 2022 Simulating continuous symmetry models with discrete ones *Phys. Rev.* B **106** 125145
[48] Sacco Shaikh D, Catalano A G, Cavaliere F, Franchini F, Sassetti M and Traverso Ziani N 2024 Towards a phase diagram of the topologically frustrated XY chain *Eur. Phys. J. Plus* **139** 743
[49] Calabrese P, Cardy J and Doyon B 2009 Special issue: entanglement entropy in extended systems *J. Phys. A: Math. Theor.* **42** 500301
[50] Affleck I, Laflorencie N and Sørensen E S 2009 Entanglement entropy in quantum impurity systems and systems with boundaries *J. Phys. A: Math. Theor.* **42** 504009
[51] Rossini D and Vicari E 2021 Coherent and dissipative dynamics at quantum phase transitions *Phys. Rep.* **936** 1
[52] Pelissetto A, Rossini D and Vicari E 2018 Out-of-equilibrium dynamics driven by localized time-dependent perturbations at quantum phase transitions *Phys. Rev.* B **97** 094414
[53] Pelissetto A, Rossini D and Vicari E 2020 Scaling properties of the dynamics at first-order quantum transitions when boundary conditions favor one of the two phases *Phys. Rev.* E **102** 012143
[54] Marič V, Giampaolo S M, Kuić D and Franchini F 2020 The frustration of being odd: how boundary conditions can destroy local order *New J. Phys.* **22** 083024
[55] Torre G, Marič V, Franchini F and Giampaolo S M 2021 Effects of defects in the XY chain with frustrated boundary conditions *Phys. Rev.* B **103** 014429
[56] Marič V, Giampaolo S M and Franchini F 2022 Fate of local order in topologically frustrated spin chains *Phys. Rev.* B **105** 064408

J. Stat. Mech. (2025) 023101